

A Hybrid NOMA-OMA Scheme for Inter-plane Intersatellite Communications in Massive LEO Constellations

Donatella Darsena, *Senior Member, IEEE*, Giacinto Gelli, *Senior Member, IEEE*, Ivan Iudice, and Francesco Verde, *Senior Member, IEEE*

Abstract—Communication between satellites in low-Earth orbit (LEO) constellations takes place through inter-satellite links (ISLs). Unlike intra-plane ISLs, which interconnect satellites belonging to the same orbital plane with fixed relative distance, inter-plane ISLs experience significant Doppler frequency shifts, since satellites belonging to different orbital planes exhibit time-varying relative distance (required, e.g., to minimize the risk of physical collisions between satellites). In this paper, we consider the problem of connecting multiple satellites, belonging to a massive LEO constellation, to a receiving satellite, referred to as the sink. Specifically, we consider a hybrid multiple access scheme, which employs a combination of non-orthogonal multiple access (NOMA), where radio-frequency ISLs share the same time-frequency resource blocks, and orthogonal multiple access (OMA), where ISLs employ orthogonal resource blocks. The set of satellites transmitting towards the sink is divided into groups, where NOMA is employed within each group, whereas OMA is used to separate different groups. Such a scheme subsumes as special cases both pure-OMA and pure-NOMA. Our study highlights that similar Doppler frequency shifts have a significant impact on the individual rates of the satellites in a pure-NOMA scheme, thus reducing the network fairness of this technique. Motivated by such a fact, we develop design strategies of the proposed hybrid NOMA-OMA scheme, which exploit inter-plane Doppler frequency diversity to enhance fairness among the satellites, while ensuring a significantly higher sum-rate capacity compared to the pure-OMA technique. Numerical results corroborate our theoretical analysis, by demonstrating both the fairness enhancement of the proposed techniques over the pure-NOMA scheme, as well as their capacity improvement over the pure-OMA one.

Index Terms—Capacity, Doppler frequency diversity, fairness, interference cancellation, low-Earth orbit (LEO) constellations,

Manuscript received December 5, 2023; revised May 22, 2024; accepted July 16, 2024. The associate editor coordinating the review of this paper and approving it for publication was Prof. Zhu Han. (*Corresponding author: Francesco Verde*)

D. Darsena, G. Gelli, and F. Verde are with the Department of Electrical Engineering and Information Technology, University Federico II, Naples I-80125, Italy [e-mail: (darsena, gelli, f.verde)@unina.it]. I. Iudice is with the Reliability & Security Department, Italian Aerospace Research Centre (CIRA), Capua I-81043, Italy (e-mail: i.iudice@cira.it).

D. Darsena, G. Gelli, and F. Verde are also with National Inter-University Consortium for Telecommunications (CNIT).

This work was partially supported by the European Union under the Italian National Recovery and Resilience Plan (NRRP) of NextGenerationEU, partnership on “Telecommunications of the Future” (PE00000001 - program “RESTART”).

This research activity falls within the field of interest of the IEEE AESS technical panel on Glue Technologies for Space Systems.

non-orthogonal multiple access (NOMA), orthogonal multiple access (OMA), resource allocation, superposition coding.

I. INTRODUCTION

THERE is an upsurge of interest, both in the industrial and academic community, towards *low-Earth orbit* (LEO) satellite constellations, whose satellites are deployed between 400 and 2000 km over the Earth surface. Compared to higher orbits, LEO constellations offer better coverage and reduced propagation delays. Such advantages have spurred standardization activities, e.g., within 3GPP, to integrate LEO satellite networks into 5G and beyond-5G networks [1], [2].

In addition to national/international public institutions, an increasing number of private companies (e.g., SpaceX, OneWeb, Amazon, and Google) have planned and started to deploy LEO constellations composed by thousands of satellites – so called *megaconstellations* – with the aim of providing global services, such as broadband Internet access and mobile telephony, as well as to support Internet-of-Remote-Things (IoRT) applications [3]. In such megaconstellations, satellites are typically organized in groups, each one following the same orbital trajectory, which lies in a plane called *orbital plane* (OP). The angle between the OP and the equatorial plane is called *inclination*, which ranges from 0° (equatorial orbits) to nearly 90° (polar orbits). For instance, the Starlink megaconstellation envisioned by SpaceX is expected to be comprised by approximately 12,000 LEO and very LEO (i.e., under 400 km) satellites, to be deployed in two phases. In phase I, SpaceX is deploying a LEO constellation of 1584 satellites, arranged in 22 orbital planes (OPs), with 72 satellites per OP, at an altitude of 550 km and an inclination of 53° .

In next-generation LEO satellite networks, in order to satisfy more challenging performance requirements, in terms of connectivity, coverage, capacity, and latency, it is commonly recognized [4] that point-to-point *intersatellite links* (ISLs) will play an important role. ISLs can be classified [4], [5] in two main categories: (1) *intra-plane*, which are established between two satellites belonging to the same OP; (2) *inter-plane*, which are established between two satellites belonging to different OPs. Moreover, inter-plane ISLs can be of three types [5]: between adjacent OPs, between nearby OPs, between crossing OPs.

0000-0000/00\$00.00 © 2024 IEEE

arXiv:2307.08340v3 [eess.SP] 19 Jul 2024

Both free-space optical (FSO) and radio-frequency (RF) communication technologies can be considered for ISL implementation [6]–[8]. The FSO solution employs very narrow beams to counteract the detrimental effects of path loss at high carrier frequencies, while assuring in principle high data-rates, large transmission ranges, and low sensitivity to interference. While optical intra-plane ISLs are easy to be established and managed, due to the slow relative motion between satellites, inter-plane optical ISLs demand significant challenges to acquisition, tracking and pointing (ATP) on-board systems, due to the ultra-narrow beamwidth of FSO links and the high relative speeds of the satellites [5]. In contrast, in inter-plane ISLs, the lower operation frequencies of radio ISL enable easier beam alignment and allow one to connect with a higher number of neighbor satellites, along with an easier integration into terrestrial RF-based networks. Among the disadvantages, radio ISLs are more susceptible to interference and provide lower data-rate compared to optical links, besides requiring a licensed bandwidth to operate. Moreover, inter-plane radio ISLs, especially those between crossing OPs, exhibit high Doppler frequency shift values, which become one of the main performance limiting factor [9]. It is worthwhile to note that the RF technology may be a reliable fallback solution when FSO links are unavailable, thereby making hybrid RF/FSO systems good candidates for inter-satellite networking [7].

For the above mentioned reasons, we will consider in the following innovative designs of inter-plane radio ISLs in a LEO network scenario. Indeed, traditional ISL designs for geostationary orbit (GEO) systems must be rethought, to be adapted to the highly dynamic features of LEO satellite networks, which are characterized by high mobility, coupled with relatively low-power transmission capabilities. Specifically, to avoid interference between ISLs caused by the sharing of RF resources by multiple communicating satellites [9], state-of-the-art satellite communications mainly adopt *orthogonal multiple access* (OMA) schemes, such as frequency-division multiple access (FDMA), time-division multiple access (TDMA), code-division multiple access (CDMA), orthogonal frequency-division multiple access (OFDMA), or combinations thereof. In recent years, *non-orthogonal multiple access* (NOMA) has been recognized [10] as a promising approach for terrestrial networks, due to its superior spectral efficiency with respect to OMA schemes. Indeed, in NOMA, multiple users are allowed to share the same time-frequency resource (or pool of resources), through power-domain or code-domain multiplexing. The superimposed signals can be separated at the receiver by using successive interference cancellation (SIC). At the cost of an increased receiver complexity, NOMA techniques offer not only improved spectral efficiency, but also fairness in some cases [11]. Spectrum efficient and secure transmission schemes for satellite communication systems have been proposed and analyzed in [12], [13], where terrestrial nodes access a satellite downlink network with frequency-division NOMA.

This paper focuses on design of hybrid NOMA-OMA multiple access strategies for inter-plane radio ISLs to be employed in LEO megaconstellations. Instead of marking ISLs with high Doppler shifts as non-feasible [9], [14], our approach opportunistically leverages the different Doppler

profiles of the satellites (so called *Doppler diversity*) to achieve a performance gain, as explained in the following.

A. Related work and open research

Some works have considered NOMA for satellite networks (see [15] and references therein), but are mainly limited to air-to-ground (downlink) or ground-to-air (uplink) communications. A power-domain NOMA scheme for the downlink of an integrated satellite-terrestrial network was considered in [3], targeted at Internet-of-Things (IoT) applications. With particular reference to LEO constellations, the performance analysis of downlink NOMA is carried out in [16], in terms of ergodic capacity, outage probability, and mutual information, by considering the case of two ground users in one spot beam. In [17], a sum-rate capacity maximization problem was considered for a LEO constellation employing massive MIMO in conjunction with NOMA. In [18], a NOMA scheme has been introduced in uplink, in the context of a multi-layer satellite networks, composed by GEO and LEO satellites. The works [3], [16]–[18] do not consider intersatellite (IS) communication at all.

The problem of IS communication has been studied in [19], where communications between two satellite groups are established with the help of a relay satellite and applying NOMA schemes for both downlink and uplink. NOMA schemes for a dual-layer LEO megaconstellation are studied in [20], aimed at allowing the coexistence of services with different requirements. However, in [19], [20], Doppler frequency shifts are regarded as a cause of performance degradation rather than as a source of diversity.

The design of ISLs for dense LEO constellations has been considered in [9], where the establishment of inter-plane ISLs is casted as a weighted dynamic matching problem and solved by performing sum-rate capacity maximization. However, this research considers an OMA scheme and, moreover, marks as *non-feasible* those links characterized by high Doppler frequency shift values. Another work in this area is [14], which deals with the problem of designing inter-plane ISLs, based on reinforcement learning, by discarding links affected by non-negligible Doppler effects.

B. Contributions

Our contributions can be summarized as follows.

- 1) We provide an accurate characterization of radio ISLs that allow multiple satellites of a LEO Walker Delta constellation to effectively communicate with a receiving satellite, referred to as the *sink*. In particular, we unveil that the satellites with feasible ISLs towards the sink belong not only to the same OP of the sink (intra-plane), but also to adjacent and crossing OPs (inter-plane), exhibiting thus significant Doppler frequency shifts.
- 2) We show that the Doppler frequency shifts characterizing inter-plane radio ISLs have a significant impact on the individual rates of the satellites that access the channel in a non-orthogonal manner with minimum mean-squared error (MMSE)-plus-SIC receiver at the sink, named as

TABLE I
MAIN PARAMETERS AND SYMBOLS (THE TIME VARIABLE t IS OMITTED).

Symbols	Meaning	Symbols	Meaning
K	number of satellites	\mathcal{L}	set of indices of feasible links
P	number of OPs	$\mathbb{P}(\mathcal{L})$	partition of \mathcal{L} (collection of satellite groups)
N	number of satellites for each OP	G	number of satellite groups
h	satellite's altitude	ρ_k	fraction of DoF allocated to \mathcal{L}_k
R	Earth's radius	$A_{\ell_k, q}$	amplitude of the link between sink and (ℓ_k, q) -th satellite
$\theta_{p, n}$	colatitude of the (p, n) -th satellite	$\tau_{\ell_k, q}$	delay of the link between sink and (ℓ_k, q) -th satellite
$\phi_{p, n}$	longitude of the (p, n) -th satellite	$\nu_{\ell_k, q}$	normalized Doppler of the link between sink and (ℓ_k, q) -th satellite
$d_{p, n}$	distance between sink and (p, n) -th satellite	T	symbol period
L	number of feasible links	T_c	sampling period
S	oversampling factor	N_0	observation interval length (in symbol periods)
$P_{p, n}^{\text{tx}}(t)$	power transmitted by the (p, n) -th satellite	$G_{p, n}^{\text{ix}}$	antenna gain of the (p, n) -th transmitting satellite
$\mathbf{r}_{p, n}(t)$	ECEF position of the (p, n) -th satellite	$G_{1, 1}^{\text{ix}}$	antenna gain of the sink satellite

pure-NOMA, which is the optimal strategy to achieve the capacity region of the considered system.

- 3) We develop design procedures of a *hybrid NOMA-OMA* scheme, where L satellites with *feasible* radio ISLs towards the sink are partitioned in groups: namely, those belonging to the same group implement NOMA, while the ones belonging to different groups employ OMA. Pure-NOMA and pure-OMA techniques are special cases of such a scheme, which are obtained by setting the number of groups equal to 1 and L , respectively. The objective of the proposed designs is to exploit the differences in Doppler frequency profiles of the superimposed satellite transmissions in order to improve system fairness, by ensuring at the same time a significant performance gain in terms of sum-rate capacity compared to the pure-OMA technique.
- 4) The performances of the considered multiple access schemes are validated numerically. It is demonstrated that exploiting of the inter-plane Doppler frequency diversity is instrumental to achieve a good trade-off between sum-rate capacity and fairness among the satellites.

This article is organized as follows. The mathematical model of the considered system and the characterization of ISLs feasibility are reported in Section II. The MMSE-SIC receiving structure at the sink is described in Section III. A comparative performance study of the pure-OMA, pure-NOMA, and hybrid NOMA-OMA schemes is carried out in Section IV, with particular emphasis on the impact of the frequency Doppler shifts. Design procedures of the proposed hybrid NOMA-OMA scheme are developed in Section V, and related numerical results are reported in Section VI. Finally, the main results obtained in this article are summarized and discussed in Section VII.

II. SYSTEM MODEL

Let us consider a general LEO Walker Delta constellation, composed of K satellites, uniformly-distributed and equally-spaced in P OPs. Each satellite follows a circular orbit around the Earth, at a given altitude h above the terrestrial surface, having an inclination α with respect to the equatorial plane, and phasing parameter F [21].

Let $N \triangleq K/P$ (assumed to be an integer) denote the number of satellites in each OP. In order to univocally identify

each satellite, we use the index pair (p, n) indicating the n -th satellite in the p -th orbital plane, for $n \in \{1, 2, \dots, N\}$ and $p \in \{1, 2, \dots, P\}$. We investigate the establishment of ISLs between a number of transmitting satellites, belonging to a group or *swarm*, towards a receiving satellite, referred to as the *sink* in the following. In particular, without loss of generality, we choose the satellite $(1, 1)$ as the communication sink. The main parameters and symbols introduced throughout the paper are summarized in Table I.

A. Conditions ensuring ISL feasibility

Herein, we investigate the problem of assuring a reliable communication link between the satellites of each group and the sink, so called *ISL feasibility*, which is influenced by the following aspects: (i) existence of line-of-sight (LoS) propagation; (ii) path loss and receiver sensitivity; (iii) satellite antenna radiation pattern.

To study the first aspect, we introduce the customary Earth-Centered Earth-Fixed (ECEF) right-handed orthogonal coordinate system (or *frame*), with origin at the center of Earth and z axis coincident with the oriented line from South pole to North pole (further details on the definition of the ECEF coordinate system are reported in Appendix A). Assuming the Earth shape to be spherical, with radius $R = 6378$ km, the position of the satellite (p, n) at the time instant $t \in \mathbb{R}$, deployed at altitude h above Earth, is defined in the ECEF frame by the spherical coordinate triple $(R + h, \theta_{p, n}(t), \varphi_{p, n}(t))$, where $\theta_{p, n}(t) \in [0, \pi]$ denotes the time-varying polar angle (or *colatitude*) and $\varphi_{p, n}(t) \in [0, 2\pi)$ denotes the time-varying azimuthal angle (or *longitude*). Therefore, the distance $d_{p, n}(t)$ at time t between the (p, n) -th satellite and the sink can be calculated with elementary geometry as

$$d_{p, n}(t) = \|\mathbf{r}_{p, n}(t) - \mathbf{r}_{1, 1}(t)\| \quad (1)$$

where $\mathbf{r}_{p, n}(t)$ is the position in the ECEF coordinate system of the n -th satellite belonging to the p -th orbit plane (see Appendix A for its definition). The corresponding ISL is in LoS visibility if condition

$$(\mathbf{c1}) : d_{p, n}(t) \leq d_{\text{horiz}} \quad (2)$$

holds, where $d_{\text{horiz}} \triangleq 2[h(h + 2R)]^{1/2}$ is the radio horizon.

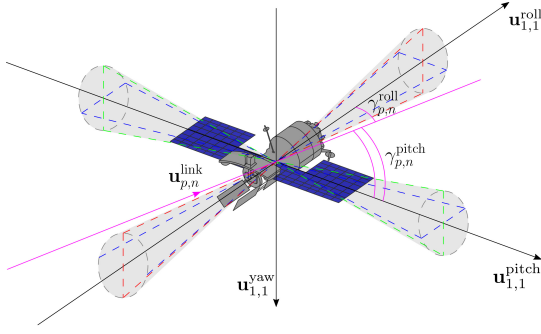


Fig. 1. The ISL antenna beams of the sink (the time variable t is omitted).

Let us consider receiver sensitivity and losses due to free-space propagation. For LEO satellites, propagation occurs mainly in the *thermosphere*, where the air molecule density is very low, hence loss mechanisms due to molecular absorption and scattering are practically absent [22]. When the signal wavelength λ_c is very small, the *geometric path loss* $(4\pi d_{p,n}(t)/\lambda_c)^2$ is considerable, so highly-directional antennas with high gains are required. Therefore, we assume that each satellite is equipped with highly-directional wide-band antennas, with approximately conical beams, whose half-beamwidths are denoted with $\beta_{p,n}$ (assumed to be equal for all the antennas on board each satellite). In this case, assuming a free-space path loss model, the received power is given by the Friis formula (see, e.g., [23])

$$P_{p,n}^{\text{rx}}(t) = P_{p,n}^{\text{tx}} G_{p,n}^{\text{tx}} G_{1,1}^{\text{rx}} \left[\frac{\lambda_c}{4\pi d_{p,n}(t)} \right]^2 \quad (3)$$

where $P_{p,n}^{\text{tx}}$ and $P_{p,n}^{\text{rx}}(t)$ are the power transmitted by the (p,n) -th satellite and received at the sink at time t , respectively, $G_{p,n}^{\text{tx}}$ and $G_{1,1}^{\text{rx}}$ represent the antenna gains of the (p,n) -th transmitting satellite and sink.¹

For the propagation link between the (p,n) -th transmitting satellite and the sink, the power $P_{p,n}^{\text{rx}}(t)$ has to fulfill the condition

$$(\mathbf{c2}) : P_{p,n}^{\text{rx}}(t) \geq P_{\text{sens}}^{\text{rx}} \quad (4)$$

where the receiver sensitivity $P_{\text{sens}}^{\text{rx}}$ represents the lowest value of the received power at which the signal can be decoded satisfactorily, i.e., with a given bit-error-rate (BER).

Finally, we take into account antenna radiation pattern limitations. Usually, a spacecraft is equipped with intra-plane ISL antennas located at both sides of the roll axis (aligned to the satellite speed vector) and inter-plane ISL antennas along the pitch axis (perpendicular to the orbit plane), as shown in Fig. 1. Hereinafter, we assume that each satellite is equipped with antennas having approximately conical beams, whose half-beamwidths $\beta_{p,n}$ are equal for all the antennas on board each satellite. Consequently, we assume that a feasible LoS link between satellite $(p,n) \neq (1,1)$ and the sink $(1,1)$ can be established only if the corresponding RF propagation direction falls within the conical antenna beams

¹In general, the antenna gains depends on t since the propagation direction is time-varying. However, in the case of highly-directional antennas, the gains can be reasonably assumed to be constant on a spherical cap.

of the sink. Mathematically, let $\gamma_{p,n}^{\text{pitch}}(t)$ and $\gamma_{p,n}^{\text{roll}}(t)$ denote the time-varying angles between $\mathbf{u}_{p,n}^{\text{link}}(t)$, i.e., the direction of propagation of the signal emitted by the (p,n) -th satellite, and the pitch and roll axes of the sink, given respectively by $\mathbf{u}_{1,1}^{\text{pitch}}(t)$ and $\mathbf{u}_{1,1}^{\text{roll}}(t)$ (see Fig. 1), the condition must hold

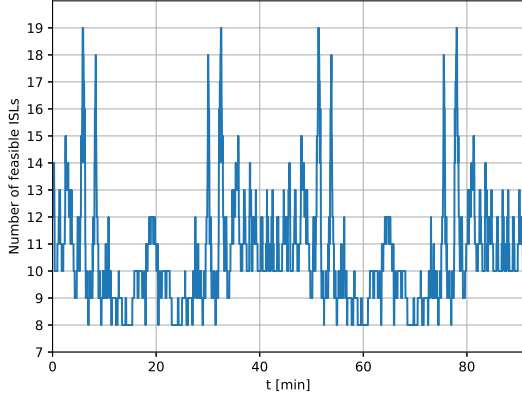
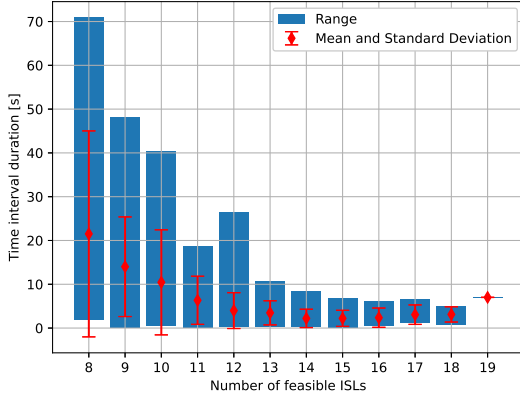
$$(\mathbf{c3}) : \{\gamma_{p,n}^{\text{pitch}}(t) \leq \beta_{1,1}\} \cup \{\gamma_{p,n}^{\text{roll}}(t) \leq \beta_{1,1}\} \text{ for } (p,n) \neq (1,1). \quad (5)$$

Definition 1 (Feasible ISLs). Only those satellites that satisfy the *three* ISL feasibility requirements **(c1)**, **(c2)**, and **(c3)**, can effectively communicate with the sink. The time-varying set $\mathcal{C}(t)$ contains all the couples (p,n) satisfying (2), (5), (4) and $L(t) \triangleq \text{card}(\mathcal{C}(t)) \leq K$ is the number of feasible ISLs.

1) *Illustrative example:* We consider a LEO Walker Delta constellation composed of $K = 1584$ satellites flying over $P = 22$ OPs at altitude $h = 550$ km. The number of satellites per OP is $N = K/P = 72$, the inclination with respect to the equatorial plane is $\alpha = 53^\circ$, and the phasing parameter (see Appendix A) is set equal to $F = 17$. Moreover, the period of revolution T_{rev} of the satellites is 91 minutes. We numerically evaluate in Fig. 2 the total number $L(t)$ of feasible ISLs as a function of t , when the sink corresponds to the satellite having indices $(15, 47)$, over a time horizon equal to T_{rev} . In this example, the signal carrier frequency $f_c = c/\lambda_c$ is 40 GHz, with c denoting the speed of light in the vacuum, the power transmitted by the satellites is $P_{p,n}^{\text{tx}} = 10$ W, the transmit and receive antenna gains are set equal to 20 dBi,² the receiver sensitivity is $P_{\text{sens}}^{\text{rx}} = -120$ dBm. It is interesting to note that the number of feasible ISLs seen by the sink over the time-scale T_{rev} exhibits a staircase trajectory, i.e., $L(t)$ remains constant over time intervals of length $\Delta_{i,\pi(i)}$, with $i \in \{8, 9, \dots, 19\}$ denoting the total number of feasible ISLs, i.e., $L(t) = i$, and $\pi(i) \in \mathbb{N}$ being the index of the time interval within $L(t)$ takes on the value i . Moreover, potential values of $L(t)$ repeat over the revolution time horizon, e.g., the value $L(t) = 19$ is taken on four times over the time-scale T_{rev} and, thus, $\pi(19) \in \{1, 2, 3, 4\}$. The minimum value of $L(t)$ is equal to 8, which corresponds to the (fixed) number of feasible intra-OP ISLs seen by the sink over each revolution time interval. Therefore, the number of feasible inter-OP ISLs varies from 1 (i.e., $i = 9$) to 11 (i.e., $i = 19$). It should be observed that, due to the periodicity of the orbits, the same result can be extended to all of the satellites of the constellation by a simple cyclic shift of the plot.

For each value of $L(t) = i$, we also show in Fig. 3 the range $[\Delta_{i,\min}, \Delta_{i,\max}]$ of $\Delta_{i,\pi(i)}$, where $\Delta_{i,\min} \triangleq \min_{\pi(i)} \Delta_{i,\pi(i)}$ and $\Delta_{i,\max} \triangleq \max_{\pi(i)} \Delta_{i,\pi(i)}$, as well as its (arithmetic) mean value and the corresponding standard deviation. It is worthwhile to note that, besides $i = 8$ representing the number of feasible intra-OP ISLs, there exist multiple inter-OP ISLs towards the sink within time windows of non-negligible length. For instance, the sink sees $i = 19$ feasible (8 intra-OP plus 11 inter-OP) ISLs over four time windows having (approximately) the same length equal to 7.025 s. A snapshot of this special case is depicted in Fig. 4.

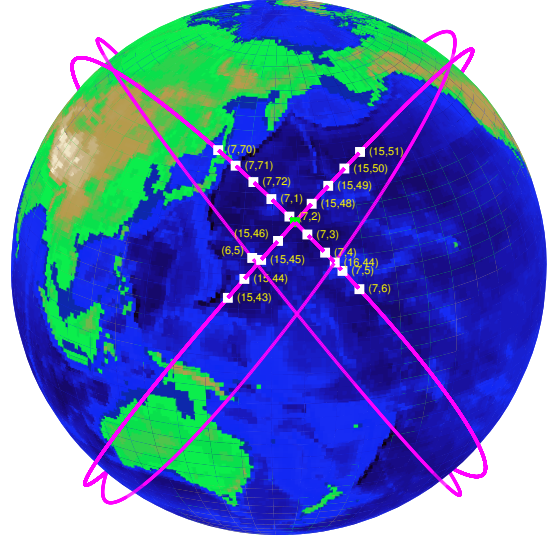
²Considering the assumptions on the antenna radiation patterns, a gain of 20 dBi roughly corresponds to 11.48 degrees half-beamwidth.


 Fig. 2. Number of feasible ISLs over the time-scale T_{rev} .

 Fig. 3. Range, mean value, and standard deviation of the time interval duration $\Delta_{i,\pi(i)}$ versus the number i of feasible ISLs over the time-scale T_{rev} .

Hereinafter, for the sake of notational simplicity, we refer to a generic time window $[0, T_0)$ of length T_0 , referred to as the *observation interval*, over which $\mathcal{C}(t)$ is constant with $L(t) \equiv L$, thus omitting the dependence of both $\mathcal{C}(t)$ and $L(t)$ on t . Moreover, it is assumed that a suitable mapping has been introduced, which transforms each two-dimensional (2D) coordinate $(p, n) \in \mathcal{C}$ into a one-dimensional (1D) index $\ell \in \mathcal{L} \triangleq \{1, 2, \dots, L\}$.

B. The proposed multiple-access transmission scheme

We briefly introduce herewith the proposed multiple-access scheme (further details are given in Sections III and IV). For a given value of $G \in \{1, 2, \dots, L\}$, let $\mathbb{P}(\mathcal{L}) = \{\mathcal{L}_k\}_{k=1}^G$ be a partition of \mathcal{L} , i.e., $\cup_{k=1}^G \mathcal{L}_k = \mathcal{L}$ and $\mathcal{L}_k \cap \mathcal{L}_h = \emptyset$ for $k \neq h$, with $\sum_{k=1}^G L_k = L$, where $L_k \triangleq \text{card}(\mathcal{L}_k)$. Our aim is to determine $\mathbb{P}(\mathcal{L})$ such that the satellites that are members of the group \mathcal{L}_k concurrently transmit by employing a NOMA scheme, based on superposition coding (SC) and SIC at the receiver, whereas the satellites belonging to different groups \mathcal{L}_k and \mathcal{L}_h , with $k \neq h$, transmit by employing an OMA scheme over non-interfering links. It is noteworthy that it is irrelevant for a capacity analysis whether the partitioning is across time or frequency (or both), since the power constraint is on the average across the degrees of freedom (DoF) [23].


 Fig. 4. A pictorial view of the $i = 19$ satellites with feasible ISLs towards the sink represented by the satellite with indices $(15, 47)$ (i.e., the green square).

We would like to recall attention to two extreme cases: when $G = 1$ and, thus, $L_1 = L$, all the L satellites with feasible links transmit over the same time-frequency resources by using the SC-SIC scheme and, in this case, one has a *pure-NOMA* technique. On the other hand, when $G = L$ and, thus, $L_k = 1$, the sink receives orthogonal signals from the L different satellites and, in this case, the proposed scheme boils down to a *pure-OMA* technique. For the intermediate values of $G \in \{2, 3, \dots, L - 1\}$, the satellites communicate with the sink through a *hybrid NOMA-OMA* transmission scheme.

C. Model of the signal received by the group \mathcal{L}_k

We assume that the partition $\mathbb{P}(\mathcal{L})$ has been determined and, without loss of generality, we focus on NOMA communication within the k -th satellite group $\mathcal{L}_k \triangleq \{\ell_{k,1}, \ell_{k,2}, \dots, \ell_{k,L_k}\}$, for $k \in \{1, 2, \dots, G\}$. Moreover, let T be the symbol period, $\{b_{\ell_{k,q}}(h)\} \in \mathbb{C}$ the sequence sent by the $(\ell_{k,q})$ -th satellite in the h -th symbol interval, with $h \in \mathbb{Z}$ and $q \in \{1, 2, \dots, L_k\}$, and let $\psi(t)$ denote the impulse response of the transmit shaping filter. With reference to a linear modulation, the baseband signal of the $(\ell_{k,q})$ -th satellite passed through the transmit shaping filter is given by

$$x_{\ell_{k,q}}(t) = \frac{1}{\sqrt{\rho_k}} \sum_{h=-\infty}^{+\infty} b_{\ell_{k,q}}(h) \psi(t - hT), \quad \text{for } t \in [0, T_0) \quad (6)$$

where ρ_k is the fraction of DoF allocated to all the satellites belonging to the group \mathcal{L}_k , with

$$\sum_{k=1}^G \rho_k = 1. \quad (7)$$

The transmitted symbols $\{b_{\ell_{k,q}}(h)\}_{h \in \mathbb{Z}}$ are modeled as mutually independent sequences of zero-mean unit-variance independent and identically distributed (i.i.d.) random variables. Hereinafter, we assume that the $(\ell_{k,q})$ -th satellite is moving (relative to the sink) at constant *radial* speed $v_{\ell_{k,q}}$ within the

observation interval. In this case, the time-varying distance covered by the wavefront transmitted by the satellite $\ell_{k,q}$ and received at the sink is given by $d_{\ell_{k,q}}(t) = d_{\ell_{k,q}}(0) + v_{\ell_{k,q}} t$, for $t \in [0, T_0)$. Under the assumption that $|v_{\ell_{k,q}}| T_0 \ll |d_{\ell_{k,q}}(0)|$, the Doppler effect induces a simple carrier frequency shift [24] and, thus, the far-field noise-free signal $r_k(t)$ received by the sink from the k -th satellite group can be expressed as

$$r_k(t) = \sum_{q=1}^{L_k} A_{\ell_{k,q}} e^{j2\pi f_{\ell_{k,q}} t} x_{\ell_{k,q}}(t - \tau_{\ell_{k,q}}) \quad (8)$$

for $t \in [0, T_0)$, where $A_{\ell_{k,q}}$, $f_{\ell_{k,q}}$, and $\tau_{\ell_{k,q}}$ are the complex amplitude, Doppler frequency shift, and delay, respectively, of the link between the $(\ell_{k,q})$ -th satellite and the sink. Model (8) has been derived under the additional assumption that $f_{k,\max} T \ll 1$, where $f_{k,\max} \triangleq \max_{q \in \{1, 2, \dots, L_k\}} |f_{\ell_{k,q}}|$ is the maximum Doppler frequency shift in \mathcal{L}_k . It should be noted that the argument of $A_{\ell_{k,q}}$ accounts for a phase misalignment between the $(\ell_{k,q})$ -th satellite and the sink.

In the following, we will assume that a timing advance (TA) scheme is employed [25], such that the signals transmitted by satellites within the same time interval arrive nearly aligned at the sink. In this case, $\tau_{\ell_{k,q}} \approx \tau_0$ in (8) and timing misalignment interference is avoided. Without loss of generality, we set hereinafter $\tau_0 = 0$ to simplify the forthcoming derivations.

At the sink, to demodulate the symbols received in the interval $[uT, (u+1)T] \subseteq [0, T_0)$ ($u \in \mathbb{Z}$), the signal (8) is first passed through a receiving filter that is matched to the transmit pulse shaping characteristic and, then, sampled with rate $1/T_c \triangleq S/T$ at instants $t_{u,s} \triangleq uT + sT_c$, for $s \in \{0, 1, \dots, S-1\}$, with $S > 1$ denoting the oversampling factor. Let $r_k^{(s)}[u] \triangleq r_k(t_{u,s})$ be the discrete-time version of (8), for $u \in \{0, 1, \dots, N_0 - 1\}$, one gets

$$r_k^{(s)}[u] = \sum_{q=1}^{L_k} \frac{A_{\ell_{k,q}}}{\sqrt{\rho_k}} e^{j2\pi S v_{\ell_{k,q}} u} e^{j2\pi v_{\ell_{k,q}} s} p(sT_c) b_{\ell_{k,q}}[u] \quad (9)$$

with $N_0 \triangleq T_0/T$ (assumed to be an integer for simplicity), the composite pulse $p(t) \triangleq \psi(t) * \psi(T-t) \approx 0 \forall t \notin (0, 2T)$,³ and $v_{\ell_{k,q}} \triangleq f_{\ell_{k,q}} T_c \in [0, 1)$ denoting the *normalized* Doppler frequency shift. Model (9) is valid under the further assumption that Doppler fluctuations vary at a very slow pace compared to the effective duration of the receiving filter.

Let $\mathbf{r}_k[u] \triangleq [r_k^{(0)}[u], r_k^{(1)}[u], \dots, r_k^{(S-1)}[u]]^T \in \mathbb{C}^S$, it results that, for $u \in \{0, 1, \dots, N_0 - 1\}$,

$$\begin{aligned} \mathbf{r}_k[u] &= \sum_{q=1}^{L_k} \frac{A_{\ell_{k,q}}}{\sqrt{\rho_k}} e^{j2\pi S v_{\ell_{k,q}} u} \tilde{\mathbf{P}} \mathbf{v}_{\ell_{k,q}} b_{\ell_{k,q}}[u] \\ &= \frac{1}{\sqrt{\rho_k}} \sum_{q=1}^{L_k} \tilde{\mathbf{h}}_{\ell_{k,q}}[u] b_{\ell_{k,q}}[u] \end{aligned} \quad (10)$$

³We have chosen a pulse shaping of finite time duration to maintain models and analysis at a reasonably simple level. Our framework can be generalized by considering other types of pulse shaping filters, e.g., the raised-cosine one.

where $\tilde{\mathbf{h}}_{\ell_{k,q}}[u] \triangleq A_{\ell_{k,q}} e^{j2\pi S v_{\ell_{k,q}} u} \tilde{\mathbf{P}} \mathbf{v}_{\ell_{k,q}} \in \mathbb{C}^S$ represents the *composite* channel response of the $(\ell_{k,q})$ -th ISL, with

$$\tilde{\mathbf{P}} \triangleq \text{diag}[p(0), p(T_c), \dots, p((S-1)T_c)] \quad (11)$$

$$\mathbf{v}_{\ell_{k,q}} \triangleq [1, e^{j2\pi v_{\ell_{k,q}}}, \dots, e^{j2\pi v_{\ell_{k,q}}(S-1)}]^T \in \mathbb{C}^S. \quad (12)$$

It should be observed that $\mathbf{v}_{\ell_{k,q}}$ is a Vandermonde vector. In the sequel, we assume that $\tilde{\mathbf{P}}$ is non-singular.

III. SIGNAL DETECTION

In this section, we describe the reception strategy adopted in the proposed NOMA scheme. We assume that the sink is perfectly aware of all channel parameters in (10), i.e., complex amplitudes $A_{\ell_{k,q}}$ and normalized Doppler frequency shifts $v_{\ell_{k,q}}$, which can be calculated from the knowledge of the deterministic motion of the satellites by means of simple geometrical arguments. This knowledge is exploited at the sink to perform simultaneous satellite symbol detection.

The overall signal received by the sink can be written as

$$\mathbf{r}[u] = \sum_{k=1}^G \mathbf{r}_k[u] + \mathbf{w}[u], \quad \text{for } u \in \{0, 1, \dots, N_0 - 1\} \quad (13)$$

where $\mathbf{w}[u] \triangleq [w^{(0)}[u], w^{(1)}[u], \dots, w^{(S-1)}[u]]^T \in \mathbb{C}^S$, with $w^{(s)}[u] \triangleq w(t_{u,s})$, and $w(t)$ represents the complex envelope of noise, modeled as a circularly-symmetric complex Gaussian random process with statistical correlation function $c_{ww}(\tau) \triangleq \mathbb{E}[w(t)w^*(t-\tau)] = \sigma_w^2 p(\tau+T)$, which is assumed to be independent of $x_{\ell_{k,q}}(t)$, for any $\ell_{k,q} \in \mathcal{L}_k$ and $k \in \{1, 2, \dots, G\}$. The positive definite correlation matrix of $\mathbf{w}[u]$ can be expressed as $\mathbf{C}_{\mathbf{w}\mathbf{w}} \triangleq \mathbb{E}[\mathbf{w}[u]\mathbf{w}^H[u]] = \sigma_w^2 \mathbf{C}_{\text{pp}}$, where the (s_1+1, s_2+1) -th entry of \mathbf{C}_{pp} is given by

$$\{\mathbf{C}_{\text{pp}}\}_{s_1+1, s_2+1} = p((s_1 - s_2)T_c + T) \quad (14)$$

for $s_1, s_2 \in \{0, 1, \dots, S-1\}$. Since \mathbf{C}_{pp} depends only on the pulse shaping waveform, it is perfectly known at the sink and, thus, the colored noise can be whitened with a whitening filter. Cholesky factorization determines the invertible whitening transformation according to $\mathbf{C}_{\text{pp}} = \mathbf{T}_{\text{pp}} \mathbf{T}_{\text{pp}}^T$, where $\mathbf{T}_{\text{pp}} \in \mathbb{R}^{S \times S}$ is a lower triangular matrix. To whiten $\mathbf{w}[u]$, the sink passes $\mathbf{r}[u]$ through the matrix multiply $\mathbf{T}_{\text{pp}}^{-1}$. By the theorem of reversibility [26], no information is lost in such a transformation. At this point, it is convenient to build a more compact vector model. In particular, let us denote with $\mathbf{b}_k[u] \triangleq [b_{\ell_{k,1}}[u], b_{\ell_{k,2}}[u], \dots, b_{\ell_{k,L_k}}[u]]^T \in \mathbb{C}^{L_k}$ the block collecting the symbols transmitted by all satellites in \mathcal{L}_k , one has from (10) and (13) that, at the output of the whitening filter, the received signal reads as

$$\bar{\mathbf{r}}[u] \triangleq \mathbf{T}_{\text{pp}}^{-1} \mathbf{r}[u] = \sum_{k=1}^G \tilde{\mathbf{H}}_k[u] \mathbf{b}_k[u] + \bar{\mathbf{w}}[u] \quad (15)$$

for $u \in \{0, 1, \dots, N_0 - 1\}$, where

$$\begin{aligned} \tilde{\mathbf{H}}_k[u] &\triangleq \frac{1}{\sqrt{\rho_k}} [\tilde{\mathbf{h}}_{\ell_{k,1}}[u], \tilde{\mathbf{h}}_{\ell_{k,2}}[u], \dots, \tilde{\mathbf{h}}_{\ell_{k,L_k}}[u]] \\ &= \frac{1}{\sqrt{\rho_k}} \mathbf{P} \mathbf{V}_k \mathbf{A}_k \mathbf{E}_k[u] \in \mathbb{C}^{S \times L_k} \end{aligned} \quad (16)$$

with $\mathbf{P} \triangleq \mathbf{T}_{\text{pp}}^{-1} \tilde{\mathbf{P}} \in \mathbb{C}^{S \times S}$ positive definite, $\mathbf{V}_k \triangleq [\mathbf{v}_{\ell_{k,1}}, \mathbf{v}_{\ell_{k,2}}, \dots, \mathbf{v}_{\ell_{k,L_k}}] \in \mathbb{C}^{S \times L_k}$ being a Vandermonde matrix, whose rank properties will be discussed soon after in Subsection III-D, whereas the diagonal matrices $\mathbf{A}_k \triangleq \text{diag}[A_{\ell_{k,1}}, A_{\ell_{k,2}}, \dots, A_{\ell_{k,L_k}}]$ and $\mathbf{E}_k[u] \triangleq \text{diag}[e^{j2\pi S\nu_{\ell_{k,1}}u}, e^{j2\pi S\nu_{\ell_{k,2}}u}, \dots, e^{j2\pi S\nu_{\ell_{k,L_k}}u}]$ are non-singular, and, finally, $\tilde{\mathbf{w}}[u] \triangleq \mathbf{T}_{\text{pp}}^{-1} \mathbf{w}[u]$.

We recall that the satellites belonging to different groups \mathcal{L}_k and \mathcal{L}_h , with $k \neq h$, transmit over point-to-point orthogonal links, which have been assigned at a system level by means of a deterministic *channel mapping* procedure. Consequently, the contribution $\tilde{\mathbf{r}}_k[u]$ of the k -th group can be perfectly recovered from (15) through a *channel demapping* operation, thus obtaining, for $u \in \{0, 1, \dots, N_0 - 1\}$,

$$\tilde{\mathbf{r}}_k[u] = \tilde{\mathbf{H}}_k[u] \mathbf{b}_k[u] + \tilde{\mathbf{w}}_k[u] \quad (17)$$

where $\tilde{\mathbf{w}}_k[u]$ is noise after the channel demapping algorithm, which is a circularly-symmetric zero-mean complex Gaussian random vector with covariance matrix $\sigma_w^2 \mathbf{I}_S$.

For each symbol period and satellite group, the detection algorithm consists of an iterative procedure with L_k iterations, which sequentially decodes each entry of $\mathbf{b}_k[u]$, by repeating the following three steps per each iteration: (i) MMSE filtering; (ii) maximum signal-to-interference-plus-noise ratio (SINR) ISL selection; (iii) SIC.

In Subsections III-A, III-B and III-C, since we focus on the u -th symbol interval and k -th group \mathcal{L}_k , we omit the dependence on both u and k for notational convenience (we maintain the subscript k only for the cardinality L_k).

A. MMSE filtering

Let $\tilde{\mathbf{r}}^{(m)} \in \mathbb{C}^S$ denote the input vector of the MMSE filter at the m -th iteration, for $m \in \{0, 1, \dots, L_k - 1\}$, where $\tilde{\mathbf{r}}^{(0)} \equiv \tilde{\mathbf{r}}$ is given by (17). As a first step, the receiver performs MMSE filtering of $\tilde{\mathbf{r}}^{(m)}$ as follows

$$\mathbf{z}^{(m)} \triangleq [z_1^{(m)}, z_2^{(m)}, \dots, z_{L_k-m}^{(m)}]^T = \tilde{\mathbf{F}}^{(m)} \tilde{\mathbf{r}}^{(m)} \quad (18)$$

which represents a soft estimate of $\mathbf{b}^{(m)} \in \mathbb{C}^{L_k-m}$, with $\mathbf{b}^{(0)} \equiv \mathbf{b}$, and $\tilde{\mathbf{F}}^{(m)} \in \mathbb{C}^{(L_k-m) \times S}$ is the solution of the MMSE problem $\min_{\tilde{\mathbf{F}}^{(m)}} \mathbb{E}[\|\tilde{\mathbf{F}}^{(m)} \tilde{\mathbf{r}}^{(m)} - \mathbf{b}^{(m)}\|^2]$, whose solution is given by

$$\tilde{\mathbf{F}}^{(m)} = \{\tilde{\mathbf{H}}^{(m)}\}^H \left[\tilde{\mathbf{H}}^{(m)} \{\tilde{\mathbf{H}}^{(m)}\}^H + \sigma_w^2 \mathbf{I}_S \right]^{-1} \quad (19)$$

where $\tilde{\mathbf{H}}^{(m)} \in \mathbb{C}^{S \times (L_k-m)}$, with $\tilde{\mathbf{H}}^{(0)} \equiv \tilde{\mathbf{H}}$. The quantities $\tilde{\mathbf{r}}^{(m)}$, $\tilde{\mathbf{H}}^{(m)}$, and $\mathbf{b}^{(m)}$ iteratively depend on $\tilde{\mathbf{r}}^{(m-1)}$, $\tilde{\mathbf{H}}^{(m-1)}$, and $\mathbf{b}^{(m-1)}$, respectively, as detailed in Subsection III-C.

B. Maximum SINR ISL selection

The maximum SINR (max-SINR) ISL selection algorithm is employed to identify, at each iteration, the ‘‘best’’ ISL, i.e., the entry of the vector $\mathbf{z}^{(m)}$ that exhibits the highest SINR at the output of the MMSE filter. To this aim, at the m -th iteration, the SINR on the ℓ -th entry of $\mathbf{z}^{(m)}$ is given [27] by

$$\text{SINR}_\ell^{(m)} = \frac{1}{\sigma_w^2 \left[\left(\sigma_w^2 \mathbf{I}_{L_k-m} + \{\tilde{\mathbf{H}}^{(m)}\}^H \tilde{\mathbf{H}}^{(m)} \right)^{-1} \right]_{\ell\ell}} - 1 \quad (20)$$

with $\ell \in \{1, 2, \dots, L_k - m\}$. Hence, at iteration m , we seek the index $\ell_{\max}^{(m)}$ that solves

$$\ell_{\max}^{(m)} = \arg \max_{\ell \in \{1, 2, \dots, L_k - m\}} \text{SINR}_\ell^{(m)} \quad (21)$$

and, thus, we get the hard estimate $\hat{b}_{\ell_{\max}^{(m)}} \triangleq \mathcal{Q}[z_{\ell_{\max}^{(m)}}^{(m)}]$ of $b_{\ell_{\max}^{(m)}}$, where $\mathcal{Q}[\cdot]$ is the minimum-distance decision metric, which depends on the constellation alphabet.

C. Successive interference cancellation

The final step of the iterative decoding algorithm consists of cancelling out, at each iteration, the contribution of $\hat{b}_{\ell_{\max}^{(m)}}$ to the remaining symbols, as

$$\tilde{\mathbf{r}}^{(m+1)} = \tilde{\mathbf{r}}^{(m)} - \hat{b}_{\ell_{\max}^{(m)}} \tilde{\mathbf{h}}_{\ell_{\max}^{(m)}}^{(m)} \quad (22)$$

where $\tilde{\mathbf{h}}_{\ell_{\max}^{(m)}}^{(m)}$ is the $[\ell_{\max}^{(m)}]$ -th column of $\tilde{\mathbf{H}}^{(m)}$. Under the simplifying assumption that $\hat{b}_{\ell_{\max}^{(m)}} \equiv b_{\ell_{\max}^{(m)}}$ (correct decision), the received vector at the $(m+1)$ -th iteration becomes

$$\tilde{\mathbf{r}}^{(m+1)} = \tilde{\mathbf{H}}^{(m+1)} \mathbf{b}^{(m+1)} + \tilde{\mathbf{w}} \quad (23)$$

where the matrix $\tilde{\mathbf{H}}^{(m+1)}$ is obtained from $\tilde{\mathbf{H}}^{(m)}$ by removing its $[\ell_{\max}^{(m)}]$ -th column and, similarly, the vector $\mathbf{b}^{(m+1)}$ is obtained from $\mathbf{b}^{(m)}$ by removing its $[\ell_{\max}^{(m)}]$ -th entry.

D. Remarks

The assumption of correct decisions is often invoked when a theoretical capacity analysis is of concern, but of course errors may be made during the SIC process: if one satellite is decoded incorrectly, all subsequent satellites in the same group are affected (so-called *error propagation* phenomenon). If all the satellites are coded with the same target error probability assuming error-free SIC, the effect of error propagation degrades the error probability by a factor of at most the number of satellites L_k [23]. This fact drives one to choose L_k reasonably small such that error propagation effects can be compensated by slightly increasing the coding block length.

As a second remark, we underline that the sum rate of the L_k satellites belonging to the k -th group \mathcal{L}_k is independent of the satellite ordering and achieves the boundary of the multiple-access channel (MAC) capacity region (see Section IV for details). However, the individual rates are affected by the satellite ordering: indeed, satellites decoded at a later stage of the SIC process can benefit from increased throughput. The maximum-SINR ordering described in Subsection III-B guarantees that satellites with better channel conditions are decoded earlier, thus allowing subsequently-decoded weaker satellites to get the best possible rate. Such a sharing strategy ensures *max-min fairness* [28].

A third remark is in order regarding the rank property of $\tilde{\mathbf{H}}_k[u]$ given by (16). Since the matrices \mathbf{P} , \mathbf{A}_k , and $\mathbf{E}_k[u]$ are non-singular, one has $\text{rank}(\tilde{\mathbf{H}}_k[u]) = \text{rank}(\mathbf{V}_k)$. Relying on the properties of Vandermonde vectors [29], one gets $\text{rank}(\mathbf{V}_k) = \min(S, L_k)$, provided that

$$\text{(c4)}: \nu_{\ell_{k,1}} \neq \nu_{\ell_{k,2}} \neq \dots \neq \nu_{\ell_{k,L_k}}. \quad (24)$$

TABLE II
DOPPLER FREQUENCY SHIFTS OF THE SATELLITES WITH FEASIBLE ISLS
TOWARDS THE SINK (15, 47).

2D index	1D index	Doppler frequency shift (Hz)
(6, 5)	1	1.082×10^6
(7, 1)	2	-1.124×10^6
(7, 2)	3	-1.138×10^6
(7, 3)	4	1.113×10^6
(7, 4)	5	1.115×10^6
(7, 5)	6	1.112×10^6
(7, 6)	7	1.106×10^6
(7, 70)	8	-1.103×10^6
(7, 71)	9	-1.111×10^6
(7, 72)	10	-1.118×10^6
(15, 43)	11	3.604×10^{-12}
(15, 44)	12	2.891×10^{-12}
(15, 45)	13	2.591×10^{-12}
(15, 46)	14	1.693×10^{-12}
(15, 48)	15	2.272×10^{-12}
(15, 49)	16	4.359×10^{-12}
(15, 50)	17	7.439×10^{-12}
(15, 51)	18	1.032×10^{-11}
(16, 44)	19	-1.258×10^9

Condition (c4) states that the Doppler frequency shifts of the satellites belonging to the k -th group \mathcal{L}_k have to be (significantly) different from each other in order to obtain a (well-conditioned) full-rank channel matrix. It is worth noticing that not all satellites with feasible ISLS towards the sink (see Definition 1) have different Doppler frequency shifts. To highlight such a fact, we have reported in Table II the Doppler frequency shifts of the $L = 19$ satellites of Fig. 4 (see also Subsection II-A1) with feasible ISLS towards the sink (15, 47) in the observation interval of duration $T_0 = 0.5$ ms (corresponding to the transmission of $N_0 = 2000$ symbols at the rate of $1/T = 4$ Mbaud). It is seen from Table II that all the eight satellites belonging to the same OP of the sink (i.e., those with $p = 15$) essentially exhibit the same Doppler frequency shift, which is very close to zero. However, the satellites that do not belong to the 15-th OP experience high Doppler frequency shifts, especially those flying over the crossing OP 7. As we will show in Section IV, this behavior has a crucial impact on the condition number of the channel matrix $\tilde{\mathbf{H}}_k[u]$ and, thus, on the design of the groups.

A final remark pertains the computational complexity of the proposed time-varying detection algorithm, which is mainly dominated by matrix inversions in (19) and (20), both involving $\mathcal{O}(S^3)$ flops to be repeated for each value of u and m . However, through straightforward manipulations, omitted here for brevity, it can be proven that $\tilde{\mathbf{F}}_k^{(m)}[u]$ can be implemented as the cascade of a time-invariant MMSE filter followed by a time-varying Doppler frequency shift compensation stage, i.e., $\tilde{\mathbf{F}}_k^{(m)}[u] = \{\mathbf{E}_k^{(m)}[u]\}^* \mathbf{F}_k$, where

$$\mathbf{F}_k \triangleq \mathbf{H}_k^H (\mathbf{H}_k \mathbf{H}_k^H + \sigma_w^2 \mathbf{I}_S)^{-1} \in \mathbb{C}^{L_k \times S} \quad (25)$$

with $\mathbf{H}_k \triangleq \mathbf{P} \mathbf{V}_k \mathbf{A}_k / \sqrt{\rho_k} \in \mathbb{C}^{S \times L_k}$ and the diagonal matrix $\mathbf{E}_k^{(m)}[u] \in \mathbb{C}^{L_k \times L_k - m}$ derived from $\mathbf{E}_k^{(m-1)}[u]$ by removing its $[j_{\max}^{(m-1)}]$ -th column, with $\mathbf{E}_k^{(0)}[u] = \mathbf{E}_k[u]$. Such a decomposition entails a reduction of the computational load in evaluating (19), since matrix inversion can be performed only

when the iterative algorithm starts and the only time-varying operation boils down to a multiplication by the diagonal matrix $\{\mathbf{E}_k^{(m)}[u]\}^*$, which is performed at each iteration. As regards SINR calculation in (20), it can be proven that (20) turns out to be time invariant and, moreover, matrix inversion can be done once, i.e., at the start of the iterative algorithm.

IV. SUM-RATE CAPACITY ANALYSIS

Assuming that the satellites encode the information using an i.i.d. Gaussian code⁴, recalled that (20) is time-invariant, the sum rate of the k -th group \mathcal{L}_k is given by

$$\mathcal{R}_k \triangleq \rho_k \sum_{m=0}^{L_k-1} \log_2 \left(1 + \text{SINR}_{k,\ell_{\max}}^{(m)} \right) \quad (\text{in bits/s/Hz}) \quad (26)$$

for $k \in \{1, 2, \dots, G\}$, where $\text{SINR}_{k,\ell}^{(m)}$ has been defined in (20) (with k omitted). After tedious but straightforward algebraic manipulations, it can be verified that

$$\begin{aligned} \mathcal{R}_k &= \rho_k \log_2 \det \left(\mathbf{I}_S + \frac{1}{\sigma_w^2} \tilde{\mathbf{H}}_k[u] \tilde{\mathbf{H}}_k^H[u] \right) \\ &= \rho_k \log_2 \det \left(\mathbf{I}_S + \frac{1}{\sigma_w^2 \rho_k} \mathbf{P} \mathbf{V}_k \mathbf{A}_k \mathbf{A}_k^* \mathbf{V}_k^H \mathbf{P}^T \right). \end{aligned} \quad (27)$$

We observe that (27) corresponds to the maximum sum rate that can be achieved by the considered system. This confirms the well-known fact that SC at the transmitters and MMSE-SIC at the receiver allow to achieve the boundary of the MAC capacity region [23]. The *sum-rate capacity* of the whole satellite system can be expressed as follows

$$\mathcal{C}_{\text{sum}} = \sum_{k=1}^G \rho_k \log_2 \det \left(\mathbf{I}_S + \frac{1}{\sigma_w^2 \rho_k} \mathbf{P} \mathbf{V}_k \mathbf{A}_k \mathbf{A}_k^* \mathbf{V}_k^H \mathbf{P}^T \right). \quad (28)$$

We provide in the following two subsections a comparative performance analysis in terms of sum-rate capacity of three different multiple access schemes, i.e., pure-NOMA, pure-OMA, and hybrid NOMA-OMA, by unveiling the crucial role played by the Doppler frequency shifts of the satellites that contend for channel resources. To this aim, for the sake of simplicity, we assume that \mathbf{P} is diagonally dominant with real nonzero diagonal entries p_0, p_1, \dots, p_{S-1} .

A. Comparison between pure-NOMA and pure-OMA schemes

Eq. (28) subsumes the sum-rate capacity of pure-NOMA and pure-OMA schemes as special cases. Indeed, the sum-rate capacity of the pure-NOMA technique can be obtained from (28) by setting $G = 1$, which implies $L_1 = L$ and $\rho_1 = 1$,

⁴If the channel input symbols are chosen from a discrete constellation, e.g., a quadrature amplitude modulation (QAM) constellation of size Q , the corresponding information rate $\mathcal{R}_k^{Q\text{-QAM}}$ is upper-bounded by \mathcal{R}_k . The rate reduction caused by the use of Q -QAM constellations depends on the SINR of the channel [30]. For high SINR values, indeed, the rate reduction may become very large since \mathcal{R}_k grows logarithmically with SINR, whereas $\mathcal{R}_k^{Q\text{-QAM}}$ is strictly upper-bounded by the logarithm of the constellation size Q . For low SINR values, instead, $\mathcal{R}_k^{Q\text{-QAM}}$ approaches \mathcal{R}_k .

i.e., NOMA is implemented among all the L satellites with feasible links, hence yielding

$$\mathcal{C}_{\text{sum}}^{\text{NOMA}} = \log_2 \det \left(\mathbf{I}_S + \frac{1}{\sigma_w^2} \mathbf{P} \mathbf{V} \mathbf{A} \mathbf{A}^* \mathbf{V}^H \mathbf{P} \right) \quad (29)$$

where $\mathbf{V} \triangleq [\mathbf{v}_1, \mathbf{v}_2, \dots, \mathbf{v}_L] \in \mathbb{C}^{S \times L}$ collects all the Vandermonde vectors associated to the L satellites and $\mathbf{A} \triangleq \text{diag}[A_1, A_2, \dots, A_L]$ gathers all the corresponding channel gains on its main diagonal. Let $\mathbf{C} \triangleq \mathbf{P} \mathbf{V} \mathbf{A} = [\mathbf{c}_1, \mathbf{c}_2, \dots, \mathbf{c}_L] \in \mathbb{C}^{S \times L}$, eq. (29) can be rewritten as follows

$$\mathcal{C}_{\text{sum}}^{\text{NOMA}} = \log_2 \det \left(\mathbf{I}_S + \frac{1}{\sigma_w^2} \sum_{\ell=1}^L \mathbf{c}_\ell \mathbf{c}_\ell^H \right). \quad (30)$$

Since the matrices \mathbf{P} and \mathbf{A} are non-singular, we underline that $\text{rank}(\mathbf{C}) = \text{rank}(\mathbf{V})$.

On the other hand, the sum-rate capacity of the pure-OMA technique can be obtained from (28) by setting $G = L$, which implies $L_k = 1$, i.e., the L satellites with feasible links access the channel in an orthogonal manner, thus obtaining

$$\mathcal{C}_{\text{sum}}^{\text{OMA}} = \sum_{\ell=1}^L \rho_\ell \log_2 \det \left(\mathbf{I}_S + \frac{1}{\sigma_w^2 \rho_\ell} \mathbf{c}_\ell \mathbf{c}_\ell^H \right). \quad (31)$$

By virtue of the matrix determinant lemma [29], eq. (31) can be equivalently rewritten as

$$\begin{aligned} \mathcal{C}_{\text{sum}}^{\text{OMA}} &= \sum_{\ell=1}^L \rho_\ell \log_2 \left(1 + \frac{\|\mathbf{c}_\ell\|^2}{\sigma_w^2 \rho_\ell} \right) \\ &= \sum_{\ell=1}^L \rho_\ell \log_2 \left(1 + \mathcal{E}_p \frac{|A_\ell|^2}{\sigma_w^2 \rho_\ell} \right) \end{aligned} \quad (32)$$

where $\mathcal{E}_p \triangleq \sum_{s=0}^{S-1} p_s^2$. It is worth noticing that, in the pure-OMA case, the sum-rate capacity does not depend on the Doppler frequency shifts of the satellites.

Since the determinant is a log-concave function on the set of positive definite matrices, it follows from Jensen's inequality applied directly to (31) that $\mathcal{C}_{\text{sum}}^{\text{OMA}} \leq \mathcal{C}_{\text{sum}}^{\text{NOMA}}$, where we have also accounted for (7). The difference between $\mathcal{C}_{\text{sum}}^{\text{NOMA}}$ and $\mathcal{C}_{\text{sum}}^{\text{OMA}}$ is *exactly* zero if \mathbf{C} has rank one, that is, $\text{rank}(\mathbf{V}) = 1$, which happens when the L satellites with feasible ISLs towards the sink (see Definition 1) have exactly the same Doppler frequency shifts, i.e., $\bar{\nu} \triangleq \nu_1 = \nu_2 = \dots = \nu_L$. Indeed, in such a particular case, it results that $\mathbf{c}_\ell = A_\ell \mathbf{P} \bar{\mathbf{v}}$, $\forall \ell \in \{1, 2, \dots, L\}$, with $\bar{\mathbf{v}} \triangleq [1, e^{j2\pi\bar{\nu}}, \dots, e^{j2\pi\bar{\nu}(S-1)}]^T \in \mathbb{C}^S$, and, thus,

$$\mathcal{C}_{\text{sum}}^{\text{OMA}} = \mathcal{C}_{\text{sum}}^{\text{NOMA}} = \log_2 \left(1 + \frac{\mathcal{E}_p}{\sigma_w^2} \sum_{\ell=1}^L |A_\ell|^2 \right) \quad (33)$$

provided that the DoF fractions of the pure-OMA scheme in (31) are chosen as

$$\rho_\ell^{\text{OMA}} = \frac{|A_\ell|^2}{\sum_{q=1}^L |A_q|^2} \quad (34)$$

for $\ell \in \{1, 2, \dots, L\}$. As intuitively expected, in the case of equal Doppler frequency shifts, the largest sum-rate capacity

is achieved with pure-OMA. However, condition $\nu_1 = \nu_2 = \dots = \nu_L$ does not hold in practice since inter-OP ISLs exhibit significantly different Doppler frequency shifts (see Table II and the discussion in Subsection III-D) and, in this context, pure-OMA is largely suboptimal in terms of sum-rate capacity.

B. Comparison between pure-NOMA and hybrid NOMA-OMA

A natural question arises about the advantage of performing a partition of the L satellites with feasible ISLs towards the sink in groups $\mathcal{L}_1, \mathcal{L}_2, \dots, \mathcal{L}_G$ over the pure-NOMA option. In this respect, let $\mathbf{C}_k \triangleq \mathbf{P} \mathbf{V}_k \mathbf{A}_k \in \mathbb{C}^{S \times L_k}$ and observe that $\mathbf{C}_1, \mathbf{C}_2, \dots, \mathbf{C}_G$ are matrices each gathering a different subset of the columns in \mathbf{C} , which will be referred to as *column matrices* of \mathbf{C} .

By using again the log-concavity of the determinant in the set of positive definite matrices, the following inequality comes from the application of the Jensen's inequality to (28):

$$\mathcal{C}_{\text{sum}} \leq \log_2 \det \left(\mathbf{I}_S + \frac{1}{\sigma_w^2} \sum_{k=1}^G \mathbf{C}_k \mathbf{C}_k^H \right) = \mathcal{C}_{\text{sum}}^{\text{NOMA}} \quad (35)$$

where we have used (7) and noticed that, since $\mathbf{C}_1, \mathbf{C}_2, \dots, \mathbf{C}_G$ are column matrices of \mathbf{C} , one has $\sum_{k=1}^G \mathbf{C}_k \mathbf{C}_k^H = \mathbf{C} \mathbf{C}^H$. Henceforth, the multiple access strategy where the L satellites are divided into groups of L_k satellites with NOMA within each group and OMA between the groups is suboptimal in terms of sum-rate capacity. Equality in (35) holds when the matrix $\mathbf{C}_k \mathbf{C}_k^H$ differs only for a scalar real constant, i.e., $\mathbf{C}_k \mathbf{C}_k^H = \chi_k \mathbf{\Omega}$, $\forall k \in \{1, 2, \dots, G\}$, which in its turn would be fulfilled in the scenario where satellites belonging to the same group \mathcal{L}_k experience the same path losses, i.e., $|A_{\ell_{k,1}}|^2 = |A_{\ell_{k,2}}|^2 = \dots = |A_{\ell_{k,L_k}}|^2 = \chi_k$, $\forall k \in \{1, 2, \dots, G\}$, and, moreover, the groups $\mathcal{L}_1, \mathcal{L}_2, \dots, \mathcal{L}_G$ gather satellites with the same Doppler frequency shifts, i.e., $\mathbf{V}_k = \mathbf{V}_{k'}$, for each $k \neq k'$. One has $\mathcal{C}_{\text{sum}} = \mathcal{C}_{\text{sum}}^{\text{NOMA}}$, provided that the DoF fractions of the hybrid NOMA-OMA scheme in (28) are chosen as $\rho_k = \chi_k / \sum_{q=1}^G \chi_q$.

The performance gain of the pure-NOMA scheme over the hybrid NOMA-OMA one comes at the price of computation complexity, which in a pure-NOMA scheme grows with the number L of satellites having feasible ISLs with respect to the sink. Moreover, the available DoF are limited by the dimension S of the observable space [23] and, thus, there is no further DoF gain beyond having S satellites performing pure-NOMA concurrently. Interestingly, there is another aspect to be accounted for the specific scenario at hand. We have seen from Table II that some satellites with feasible ISLs towards the sink have the same Doppler frequency shift. Therefore, *what happens if there exist satellites with the same Doppler frequency shift that access the channel by using the pure-NOMA scheme?* According to (35), the pure-NOMA technique ensures the best possible sum-rate capacity even in this particular case. However, *what are the individual rates of the satellites with the same Doppler frequency shifts?* To give an answer, let us consider the two-satellite example, where the received signal (17) at the sink ends up to

$$\bar{\mathbf{r}}[u] = \tilde{\mathbf{h}}_1[u] b_1[u] + \tilde{\mathbf{h}}_2[u] b_2[u] + \bar{\mathbf{w}}[u] \quad (36)$$

with $\tilde{\mathbf{h}}_\ell[u] \triangleq A_\ell e^{j2\pi S \nu_\ell u} \mathbf{P} \mathbf{v}_\ell \in \mathbb{C}^S$, for $\ell \in \{1, 2\}$ (the dependence on the group index k has been omitted since $G = 1$ in the pure-NOMA scheme). Assuming without loss of generality that satellite 1 is canceled first, the individual rates of the two satellites are given by $\mathcal{R}_\ell = \log_2(1 + \text{SINR}_\ell)$ (in bits/s/Hz), for $\ell \in \{1, 2\}$, where, starting from (20), after some algebraic manipulations, one has

$$\text{SINR}_1 \triangleq \frac{\sigma_w^2 |A_1|^2 \mathcal{E}_p + |A_1|^2 |A_2|^2 \left(\mathcal{E}_p^2 - |\mathbf{v}_1^H \mathbf{P}^2 \mathbf{v}_2|^2 \right)}{\sigma_w^2 (|A_2|^2 \mathcal{E}_p + \sigma_w^2)} \quad (37)$$

$$\text{SINR}_2 \triangleq |A_2|^2 \frac{\mathcal{E}_p}{\sigma_w^2} \quad (38)$$

with

$$|\mathbf{v}_1^H \mathbf{P}^2 \mathbf{v}_2|^2 = \left| \sum_{s=0}^{S-1} p_s^2 e^{-j2\pi s(\nu_1 - \nu_2)} \right|^2 \leq \mathcal{E}_p^2. \quad (39)$$

Equality in (39) holds when the two satellites have the same Doppler frequency shift, i.e., $\nu_1 = \nu_2$. Hence, we can infer

$$\text{SINR}_1 \geq \text{SINR}_1^{\min} \triangleq \frac{|A_1|^2}{|A_2|^2 + \frac{\sigma_w^2}{\mathcal{E}_p}} \quad (40)$$

where SINR_1^{\min} is the SINR of satellite 1 in the case when the Doppler frequency shifts are equal. Two interesting conclusions can be drawn from (40). First, if the two satellites have different Doppler frequency shifts, i.e., $\nu_1 \neq \nu_2$, the satellite that is decoded first can benefit of a larger rate, compared to the case when $\nu_1 = \nu_2$. Second, in the high signal-to-noise ratio (SNR) regime, i.e., as $\mathcal{E}_p/\sigma_w^2 \rightarrow +\infty$, the rate of satellite 2 increases without bound, whereas the rate of satellite 1 tends approximately to 1 bit/s/Hz when, besides having the same Doppler frequency shift, the satellites experience comparable path losses, i.e., $|A_1| \approx |A_2|$.

In a nutshell, even though the pure-NOMA scheme exhibits the highest sum-rate capacity, it might result in a very unfair resource allocation, since basically the satellites having different Doppler frequency shifts might be allowed to achieve higher data rates with respect to those exhibiting equal Doppler frequency shifts. This suggests that, compared to the pure-NOMA scheme, the hybrid NOMA-OMA strategy may better capture fairness among satellites by judiciously partitioning them in groups on the basis of their Doppler frequency shifts, without appreciably degrading the sum-rate capacity. Next section studies such an insight in greater detail.

V. OPTIMIZATION OF THE HYBRID NOMA-OMA SCHEME

Along the same lines of Subsection III-D, we observe that $r_k \triangleq \text{rank}(\mathbf{C}_k) = \text{rank}(\mathbf{V}_k) \leq \min(S, L_k)$, where the equality holds if condition (24) is fulfilled, i.e., the Doppler frequency shifts of the satellites belonging to \mathcal{L}_k are distinct. Let $\mu_{k,1} \geq \mu_{k,2} \geq \dots \geq \mu_{k,r_k} > 0$ be the nonzero singular values of \mathbf{C}_k , eq. (28) can be written as

$$\mathcal{C}_{\text{sum}} = \sum_{k=1}^G \sum_{s=1}^{r_k} \rho_k \log_2 \left(1 + \frac{\mu_{k,s}^2}{\sigma_w^2 \rho_k} \right) \quad (41)$$

which shows that all the available per-group DoF can be exploited when r_k reaches its maximum value, given by $\min(S, L_k)$, i.e., the Doppler frequency shifts of the satellites belonging to \mathcal{L}_k are distinct, for each $k \in \{1, 2, \dots, G\}$. Consequently, we impose by design that the partition $\mathbb{P}(\mathcal{L})$ obeys $r_k = \min(S, L_k)$.

There are two design issues of the hybrid NOMA-OMA scheme to be faced with: (i) distribution of the available DoF among the satellites having feasible ISLs with respect to the sink, i.e., optimization of the variables $\rho_1, \rho_2, \dots, \rho_G$, subject to constraint (7); (ii) choice of the partition $\mathbb{P}(\mathcal{L})$, i.e., setting of G and definition of the satellite groups $\mathcal{L}_1, \mathcal{L}_2, \dots, \mathcal{L}_G$, subject to constraint $r_k = \min(S, L_k)$. Such optimization objectives are coupled to each other as shown soon after.

As a first step, by using the product rule of logarithms, we equivalently rewrite (41) as follows

$$\mathcal{C}_{\text{sum}} = \sum_{k=1}^G \rho_k \log_2 \left(\prod_{s=1}^{r_k} \left[1 + \frac{\mu_{k,s}^2}{\sigma_w^2 \rho_k} \right] \right). \quad (42)$$

As a second step, by invoking the arithmetic-geometric mean inequality for non-negative real numbers [29], one obtains the following upper bound:

$$\mathcal{C}_{\text{sum}} \leq \sum_{k=1}^G r_k \rho_k \log_2 \left(1 + \frac{1}{\sigma_w^2 \rho_k} \left[\frac{1}{r_k} \sum_{s=1}^{r_k} \mu_{k,s}^2 \right] \right) \quad (43)$$

with equality if and only if the nonzero singular values of \mathbf{C}_k are all equal, i.e., the (spectral) condition number $\kappa(\mathbf{C}_k) \triangleq \mu_{k,1}/\mu_{k,r_k}$ is equal to 1 [29], for each $k \in \{1, 2, \dots, G\}$. The upper bound in (43) cannot be achieved in practice since $\kappa(\mathbf{C}_k) = 1$ if and only if $\mathbf{C}_k \mathbf{C}_k^H \propto \mathbf{I}_S$ and $S \leq L_k$ or $\mathbf{C}_k^H \mathbf{C}_k \propto \mathbf{I}_{L_k}$ and $S \geq L_k$. Henceforth, for the problem at hand, $\kappa(\mathbf{C}_k) > 1$ and, to maximize the sum-rate capacity, the design objective of the satellite groups is to ensure that $\mathbf{C}_1, \mathbf{C}_2, \dots, \mathbf{C}_G$ have condition numbers as close to 1 as possible. Moreover, recalling that the available DoF are limited by S , we design the partition $\mathbb{P}(\mathcal{L})$ such that each group has a number of satellites L_k smaller than or equal to S , i.e., we impose that $r_k = \min(S, L_k) = L_k$, for each $k \in \{1, 2, \dots, G\}$. To summarize, we came up with the following guideline for the design of the satellite groups $\mathcal{L}_1, \mathcal{L}_2, \dots, \mathcal{L}_G$.

Guideline D_g (Design of satellite groups): $\forall k \in \{1, 2, \dots, G\}$, form the group \mathcal{L}_k by selecting from the set \mathcal{L} , which gathers all the satellites with feasible ISLs towards the sink, L_k satellites such that:

- their Doppler frequency shifts are distinct, i.e., $r_k = \text{rank}(\mathbf{C}_k) = L_k$;
- $\kappa(\mathbf{C}_k)$ is close to 1 as possible.

The reformulation of the guideline D_g in terms of an algorithm with manageable complexity is pursued in Subsection V-A. For the time being, let us assume that D_g has been fulfilled such that we can regard the upper bound in (42) as a sharp approximation of the sum-rate capacity, i.e.,

$$\mathcal{C}_{\text{sum}} \approx \sum_{k=1}^G L_k \rho_k \log_2 \left(1 + \frac{1}{\sigma_w^2 L_k \rho_k} \sum_{s=1}^{L_k} \mu_{k,s}^2 \right). \quad (44)$$

Given the group sizes L_1, L_2, \dots, L_G , with $\sum_{k=1}^G L_k = L$, the problem of finding the values of the DoF fractions $\rho_1, \rho_2, \dots, \rho_G$, for which the approximation (44) of \mathcal{C}_{sum} is maximized, subject to (7), does not admit a closed-form solution. For such a reason, as a third step, we resort to a max-min approach. Specifically, we propose to maximize with respect to $\rho_1, \rho_2, \dots, \rho_G$, subject to (7), the lower bound

$$\mathcal{C}_{\text{sum}} \gtrsim L_{\min} \sum_{k=1}^G \rho_k \log_2 \left(1 + \frac{1}{\sigma_w^2 L_k \rho_k} \sum_{s=1}^{L_k} \mu_{k,s}^2 \right). \quad (45)$$

with $L_{\min} \triangleq \min_{k \in \{1, 2, \dots, G\}} L_k$, where the approximation holds when the satellite groups have the same cardinality, i.e., L_k is independent of k . By Jensen's inequality [29], we have

$$\begin{aligned} \sum_{k=1}^G \rho_k \log_2 \left(1 + \frac{1}{\sigma_w^2 L_k \rho_k} \sum_{s=1}^{L_k} \mu_{k,s}^2 \right) \\ \leq \log_2 \left(1 + \frac{1}{\sigma_w^2} \sum_{k=1}^G \frac{1}{L_k} \sum_{s=1}^{L_k} \mu_{k,s}^2 \right) \end{aligned} \quad (46)$$

where the upper bound is achieved when the DoF fractions are chosen as follows

$$\rho_k^{\text{hybrid}} = \frac{\frac{1}{L_k} \sum_{s=1}^{L_k} \mu_{k,s}^2}{\sum_{q=1}^G \frac{1}{L_q} \sum_{s=1}^{L_q} \mu_{q,s}^2} \quad (47)$$

for $k \in \{1, 2, \dots, G\}$, which represent the solution of the proposed max-min problem. Having dealt with design issue (i), we provide in the forthcoming subsection a solution of issue (ii) according to D_g .

A. Choice of the satellite groups

Preliminarily, we observe that, since \mathbf{P} and \mathbf{A}_k are diagonal non-singular matrices, and \mathbf{V}_k is full rank under guideline D_g , one has

$$\begin{aligned} 1 < \kappa(\mathbf{C}_k) &\leq \kappa(\mathbf{P}) \kappa(\mathbf{V}_k) \kappa(\mathbf{A}_k) \\ &= \frac{p_{\max}}{p_{\min}} \frac{A_{k,\max}}{A_{k,\min}} \kappa(\mathbf{V}_k) \end{aligned} \quad (48)$$

with $p_{\min} \triangleq \min_{s \in \{0, 1, \dots, S-1\}} |p_s|$, $p_{\max} \triangleq \max_{s \in \{0, 1, \dots, S-1\}} |p_s|$, $A_{k,\min} \triangleq \min_{q \in \{1, 2, \dots, L_k\}} |A_{\ell_{k,q}}|$, $A_{k,\max} \triangleq \max_{q \in \{1, 2, \dots, L_k\}} |A_{\ell_{k,q}}|$. We note that p_{\min} and p_{\max} depend on the choice of the pulse-shaping filter $p(t)$ and sampling period T_c , and are not functions of k . On the other hand, $A_{k,\min}$ and $A_{k,\max}$ depend on the geometric path losses of the satellites belonging to the group \mathcal{L}_k , and they do not depend on the corresponding phase misalignments. The condition number of the Vandermonde matrix \mathbf{V}_k depends on the Doppler frequency shifts of the satellites belonging to \mathcal{L}_k .⁵ Since the singular values of a matrix are continuously depending on its entries, we expect that $\kappa(\mathbf{V}_k)$ grows if such

⁵If the Doppler frequency shifts in \mathcal{L}_k lay on a fixed grid with width $1/S$ when $S \geq L_k$, then one would have a perfectly conditioned Vandermonde matrix, i.e., $\kappa(\mathbf{V}_k) = 1$.

Doppler frequency shifts become close to each other. To characterize such a behavior, a meaningful notion of distance between the Doppler frequency shifts is necessary. Since \mathbf{V}_k is a Vandermonde matrix on the unit circle, we can resort to the (normalized) arc length between points on the unit circle.

Definition 2 (Wrap-around distance). For $k \in \{1, 2, \dots, G\}$, let us define the *Doppler frequency shift set* $\mathcal{D}_k \triangleq \{\nu_{\ell_{k,1}}, \nu_{\ell_{k,2}}, \dots, \nu_{\ell_{k,L_k}}\}$ of the k -th satellite group \mathcal{L}_k . The wrap-around distance between two Doppler frequency shifts $\nu_{\ell_{k,q}}, \nu_{\ell_{k,q'}} \in \mathcal{D}_k$ is defined as follows

$$|\nu_{\ell_{k,q}} - \nu_{\ell_{k,q'}}|_{\mathcal{D}_k} \triangleq \min_{\eta \in \mathbb{Z}} |\nu_{\ell_{k,q}} - \nu_{\ell_{k,q'}} + \eta|. \quad (49)$$

The *minimal separation distance* δ_k of the Doppler frequency shift set \mathcal{D}_k is given by

$$\delta_k \triangleq \min_{\substack{\nu_{\ell_{k,q}}, \nu_{\ell_{k,q'}} \in \mathcal{D}_k \\ \nu_{\ell_{k,q}} \neq \nu_{\ell_{k,q'}}}} |\nu_{\ell_{k,q}} - \nu_{\ell_{k,q'}}|_{\mathcal{D}_k}. \quad (50)$$

It should be noted that, under assumption $f_{k,\max} T \ll 1$ (see Subsection II-C), it follows that $\delta_k \ll 1/S$, i.e., the Doppler frequency shifts in \mathcal{D}_k are *nearly colliding*. Inequality (48) and Definition 2 suggest the following reformulation of D_g .

Guideline D_g (Reformulation): $\forall k \in \{1, 2, \dots, G\}$, form the group \mathcal{L}_k by selecting from the set \mathcal{L} , which gathers all the satellites with feasible ISLs towards the sink, L_k satellites such that:

- their Doppler frequency shifts are distinct, i.e., $r_k = \text{rank}(\mathbf{C}_k) = L_k$;
- the minimal separation distance δ_k is maximized;
- their path losses are comparable, i.e., $A_{k,\max} \approx A_{k,\min}$.

On the basis of the discussion carried out in Subsection IV-B, the first two requirements (i.e., $\text{rank}(\mathbf{C}_k) = L_k$ and maximization of δ_k) avoid an unfair resource allocation within the group \mathcal{L}_k . Since the individual rates of the satellites also depend on their corresponding path losses, the third requirement $A_{k,\max} \approx A_{k,\min}$ goes on the direction of improving fairness among satellites belonging to the same group, too.

A strictly exhaustive procedure for finding the partition $\mathbb{P}(\mathcal{L})$ according to D_g is often computationally unmanageable, even for small values of L . In the subsequent two subsections, we propose two algorithms: in the former one, referred to as *Doppler-based partitioning*, we propose to partition the satellites into groups with the aim of creating high Doppler heterogeneity within each group and high Doppler similarity between groups (*anticlustering*), thus accounting for the first two requirements of D_g , without however considering the third requirement in terms of path losses; in the latter one, referred to as *max-fairness partitioning*, we propose to maximize a global fairness index, which implicitly accounts for all the three requirements of D_g , through an exhaustive search in suitably-reduced search space.

1) *Doppler-based partitioning*: Anticlustering consists of maximizing instead of minimizing a clustering objective function [31], [32]. For Doppler-based partitioning, we aim

Algorithm 1: Doppler-based partitioning and subsequent DoF fraction assignment.

Input quantities: The set \mathcal{L} of the L satellites with feasible ISLs towards the sink within the considered observation interval and their corresponding Doppler frequency shifts f_1, f_2, \dots, f_L .

Output quantities: The partition $\mathbb{P}(\mathcal{L}) = \{\mathcal{L}_k\}_{k=1}^G$ of \mathcal{L} .

1. Set G equal to the number of satellites belonging to the same OP of the sink (they have equal Doppler frequency shifts very close to zero) and arbitrarily assign satellites to the G anticlusters by ensuring that each anticluster consists of (approximately) the same number of satellites.
 2. Select the first satellite and check how (51) will change if the selected item is swapped with each satellite that is currently assigned to a different anticluster.
 3. After performing each possible swap, realize the one that entails the most significant increase of (51). No swap is realized if the objective cannot be improved.
 4. The procedure terminates when the swap operation has been repeated for each satellite.
 5. Assign the DoF fractions to each group according to (47) (*optimized DoF assignment*) or set $\rho_k^{\text{hybrid}} = 1/G$ (*uniform DoF assignment*).
-

at maximizing the variance among Doppler features of the satellites with feasible ISLs towards the sink (so-called *k-means anticlustering*). Specifically, we propose to determine the partition $\mathbb{P}(\mathcal{L})$ by maximizing the cost function:

$$\mathcal{V}(\mathcal{L}_1, \mathcal{L}_2, \dots, \mathcal{L}_G) \triangleq \sum_{k=1}^G \sum_{q=1}^{L_k} (f_{\ell_{k,q}} - \bar{f}_k)^2 \quad (51)$$

where $\bar{f}_k \triangleq \frac{1}{L_k} \sum_{q=1}^{L_k} f_{\ell_{k,q}}$ is the *cluster centroid* of the k -th group. It is shown in [33] that there is a direct connection between $\mathcal{V}(\mathcal{L}_1, \mathcal{L}_2, \dots, \mathcal{L}_G)$ and the location of the cluster centroids. If the cost function (51) is maximal, the cluster centroids are as close as possible to the overall centroid

$$\bar{f} \triangleq \frac{1}{L} \sum_{k=1}^G \sum_{q=1}^{L_k} f_{\ell_{k,q}} \quad (52)$$

and, therefore, to each other [33]. Thus, *k-means anticlustering* directly optimizes the similarity of the mean attribute values between clusters. Unfortunately, finding a partitioning that maximizes Doppler heterogeneity according to this criterion is still computationally challenging (i.e., it can be shown to be NP-hard). Indeed, the number of anticlustering partitions increases exponentially with L , quickly rendering it impossible to find them all out in acceptable running time. For such a reason, we propose a low-complexity solution, which is based on a swap-based heuristic [34].

Our heuristic algorithm is based on swapping satellites between anticlusters such that each swap improves the ob-

jective function (51) by the largest possible margin. The proposed algorithm is summarized as Algorithm 1 at the top of next page. It can be shown [34] that Algorithm 1 performs very similarly to exact solution methods, e.g., integer linear programming, which ensure global optimal solution at the price of an exponential explosion of the running time even for small values of L . However, Algorithm 1 does not explicitly account for system fairness and the partition is determined without accounting for the available DoF.

2) *Max-fairness partitioning:* A simple yet informative index to quantify the fairness of a scheduling scheme was proposed in [35], which, according to (26), is given by (53). If all the L satellites get the same rate, then the fairness index is 1 and the multiple access method is said to be 100% fair. On the other hand, a multiple access scheme that favors only a few selected users has a fairness index tending to 0.

We propose to maximize (53) by resorting to a *reduced* exhaustive search. The possible partitions of the set \mathcal{L} is the Bell number $B_L = \frac{1}{e} \sum_{i=0}^{+\infty} \frac{i^L}{i!}$.⁶ For the example of Fig. 4, the size of the set \mathcal{L} is $L = 19$ and, in this case, there are $B_{19} = 5.832.742.205.057$ partitions to be generated and tested. To reduce the set of candidate partitions to a manageable size, the proposed procedure is based on a problem-specific preprocessing step that we call *prepartitioning*. In the prepartitioning step, we preliminarily identify the satellites that exhibit Doppler frequency shifts that are as similar as possible, by exploiting constellation network information. Specifically, according to Table II (see also Subsection III-D), we know that the satellites with feasible ISLs belonging to the same OP of the sink are characterized by Doppler frequency shifts almost equal to zero. Such satellites are assigned to different G groups and, thus, they operate according to the OMA scheme. So doing, the problem boils down to assign the remaining $L - G$ satellites to the G groups such that to maximize (53), whose number of possible partitions is given by G^{L-G} . In the case of Fig. 2 (see also Table II), one has $G = 8$ and, hence, there are $8^{19-8} = 8.589.934.592$ candidate partitions, which can be generated and tested in a reasonable running time. The proposed algorithm is summarized as Algorithm 2 at the top of this page. It is noteworthy that Algorithm 2 jointly performs partitioning and DoF assignment to the satellite groups.

Remark: Algorithms 1 and 2 can be implemented in a full LEO context-aware and reconfigurable architecture [36]–[38], where each satellite is capable of collecting information from the neighboring ones. Specifically, by relying on the knowledge of the relative positions of the satellites as well as on the characteristics of the receiver equipment, each satellite can build a *feasibility map* - which can be calculated offline - containing the time windows over which it can establish a feasible communication link with other neighboring satellites. Standard Request-to-Send (RTS) and Clear-to-Send (CTS) mechanisms can be employed to setup the communication links between the relevant satellites and the sink.

⁶It can be interpreted as the L -th moment of a Poisson distribution with expected value 1.

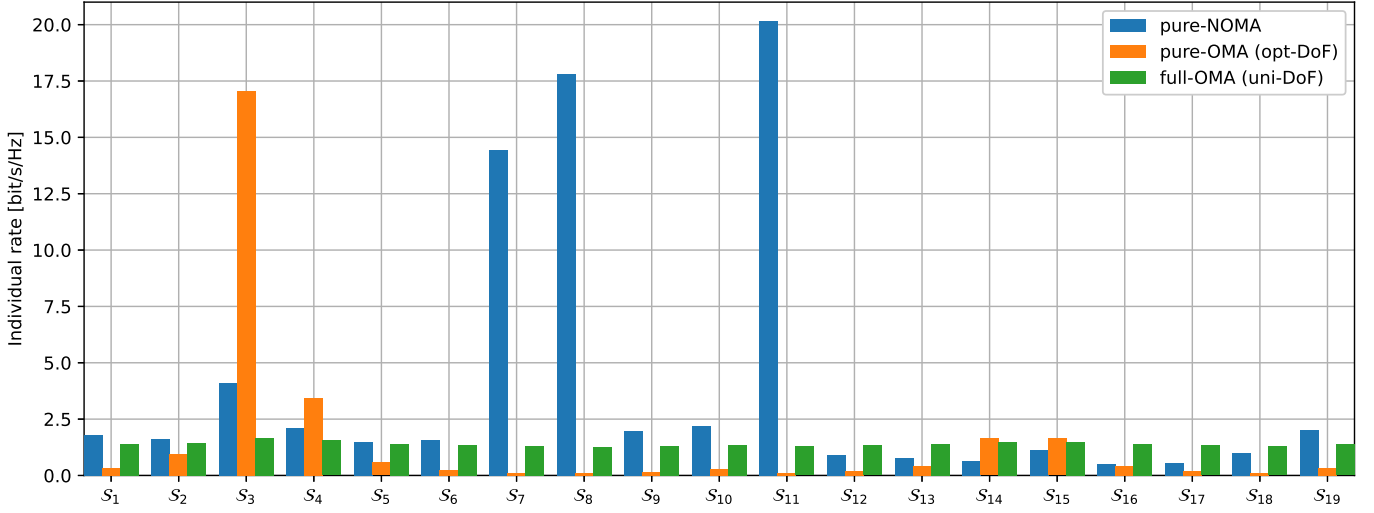


Fig. 5. Individual rates of the $L = 19$ satellites with feasible ISLs towards the sink of pure-NOMA and pure-OMA schemes.

$$\mathcal{F}(\mathcal{L}_1, \mathcal{L}_2, \dots, \mathcal{L}_G) \triangleq \frac{\left[\sum_{k=1}^G \sum_{m=0}^{L_k-1} \rho_k \log_2 \left(1 + \text{SINR}_{k, \ell_{\max}^{(m)}}^{(m)} \right) \right]^2}{L \sum_{k=1}^G \sum_{m=0}^{L_k-1} \left[\rho_k \log_2 \left(1 + \text{SINR}_{k, \ell_{\max}^{(m)}}^{(m)} \right) \right]^2}. \quad (53)$$

VI. NUMERICAL RESULTS

In this section, we provide numerical results aimed at corroborating the developed performance analysis and comparing the performance of the three multiple access schemes, namely, pure-OMA, pure-NOMA, and hybrid NOMA-OMA. To this aim, with reference to an observation interval of length 0.5 ms, we consider the same simulation setting used to generate Fig. 4 and Table II (see Subsections II-A1 and III-D for details). We recall that, in this scenario, the number of satellites with feasible ISLs towards the sink is $L = 19$, which, according to Figs. 2 and 3, represents the more challenging application from the MAC viewpoint.⁷

Unless otherwise specified, the receiving device at the sink is affected by thermal noise with a noise figure F of 8 dB and the oversampling factor at the sink is $S = 8$. As performance metrics, we consider both the sum-rate capacity and the fairness index (53).

With reference to the pure-OMA scheme, we report the performance when DoF fractions are chosen according to (34), referred to as “pure-OMA (opt-DoF)”, as well as when they are allocated uniformly, i.e. $\rho_1 = \rho_2 = \dots = \rho_L = 1/L$, referred to as “pure-OMA (uni-DoF)”. In a similar way, we implement the two versions of the proposed hybrid NOMA-OMA technique optimized as in Algorithms 1 and 2 by assigning the DoF fractions in accordance with both (47), referred to as “hyb-NOMA-OMA-1 (opt-DoF)” and “hyb-NOMA-OMA-2 (opt-DoF)”, respectively, and the uniform

rule $\rho_1 = \rho_2 = \dots = \rho_G = 1/G$, referred to as “hyb-NOMA-OMA-1 (uni-DoF)” and “hyb-NOMA-OMA-2 (uni-DoF)”, respectively.

Algorithm 2: Max-fairness joint partitioning and DoF fraction assignment.

Input quantities: The set \mathcal{L} of the L satellites with feasible ISLs towards the sink within the considered observation interval and their corresponding Doppler frequency shifts f_1, f_2, \dots, f_L .

Output quantities: The partition $\mathbb{P}(\mathcal{L}) = \{\mathcal{L}_k\}_{k=1}^G$ of \mathcal{L} .

1. Individuate the G satellites $\{\ell_{1,1}, \ell_{2,1}, \dots, \ell_{G,1}\} \subset \mathcal{L}$ that belong to the same OP of the sink (they have equal Doppler frequency shifts very close to zero) and perform the prepartitioning $\mathcal{L}_1 = \{\ell_{1,1}\}, \mathcal{L}_2 = \{\ell_{2,1}\}, \dots, \mathcal{L}_G = \{\ell_{G,1}\}$.
 2. Generate a candidate solution by assigning the remaining $L - G$ satellites to the G group.
 3. Assign the DoF fractions to each candidate group according to (47) (*optimized DoF assignment*) or set $\rho_k^{\text{hybrid}} = 1/G$ (*uniform DoF assignment*).
 4. Evaluate the fairness index (53).
 5. After performing Steps 2, 3, and 4 for all the possible partitions, choose the one that maximizes (53).
-

Fig. 5 reports the individual rates of all the satellites $\{\mathcal{S}_\ell\}_{\ell=1}^L$ with feasible ISLs towards the sink of the pure-NOMA and pure-OMA schemes. On the other hand, the

⁷Results not reported here for the lack of space show that similar conclusions can be drawn for other values of L reported in Fig. 2.

TABLE III
SUM-RATE CAPACITY AND FAIRNESS INDEX OF ALL OF THE ANALYZED
SCHEMES FOR $F = 8$ DB.

Algorithm	C_{sum}	\mathcal{F}
pure-NOMA	76.645	0.316
pure-OMA (opt-DoF)	28.237	0.136
pure-OMA (uni-DoF)	26.409	0.995
Alg. 1 (opt-DoF)	61.697	0.384
Alg. 2 (opt-DoF)	58.065	0.800
Alg. 1 (uni-DoF)	53.100	0.954
Alg. 2 (uni-DoF)	54.856	0.997

individual rates of all the satellites with feasible ISLs towards the sink of the hybrid NOMA-OMA schemes are shown in Fig. 6. The corresponding synthetic parameters, i.e., the sum-rate capacity and the fairness index, of all of the considered multiple access schemes are summarized in Table III. It is seen that, besides significantly outperforming the pure-OMA technique in terms of sum-rate capacity (see Subsection IV-A), the pure-NOMA scheme also ensures a better fairness among the satellites when the pure-OMA DoF fractions are chosen as in (34). This is in accordance with [11]. If the pure-OMA DoF fractions are allocated uniformly, the sum-rate capacity of the pure-OMA scheme further cuts down but, however, it becomes almost 100% fair. Corroborating the analysis of Subsection IV-B, the results of Table III confirm the fact that, even though it is optimal in an information-theoretical sense, the pure-NOMA schemes is quite unfair when the transmissions of satellites with similar Doppler frequency shifts are superimposed.

Table III also highlights that Alg. 1 (opt-DoF), which performs a Doppler-based partitioning by using (47), substantially ensures the same fairness index of the pure-NOMA scheme. However, when the hybrid NOMA-OMA scheme is designed by using Algorithm 1 with uniform DoF fractions, Alg. 1 (uni-DoF) is as fair as pure-OMA (uni-DoF), by remarkably assuring a sum-rate capacity increase of about 27 bits/s/Hz. Algorithm 2 allows the hybrid NOMA-OMA scheme to enhance network fairness at the price of a slight reduction of the sum-rate capacity compared to Alg. 1 (opt-DoF) and Alg. 1 (uni-DoF). For instance, Alg. 1 (opt-DoF) enhances the fairness index of 50% with respect to pure-NOMA scheme, while outperforming pure-OMA (opt-DoF) of about 30 bits/s/Hz, which is the best trade-off between fairness and information rate for the methods under comparison.

Table IV gathers the partitions found by the different algorithms. It should be remembered that the partition provided by Algorithm 1 does not depend on the DoF fractions and, thus, Alg. 1 (opt-DoF) and Alg. 1 (uni-DoF) return the same partitions. It can be observed that the number of groups is $G = 8$, which is exactly the number of satellites with feasible ISLs belonging to the same OP of the sink (see Table II). Moreover, it is noteworthy that the proposed algorithms ensure a reasonable small number of satellites for each group, which allows to compensate error propagation effects of practical implementations of the SIC process by slightly increasing the coding block length (see also Subsection III-D).

Figs. 7 and 8 depict the sum-rate capacity and the fairness index of the schemes under comparison as a function of the

oversampling factor S at the sink. It can be argued that S has a large impact on the sum-rate capacity of the NOMA-based schemes, whereas the rate performance of the OMA-based techniques slightly improves for increasing values of S . In particular, the sum-rate capacity of hyb-NOMA-OMA-1 (opt-DoF) tends to diminish when the oversampling rate at the sink becomes greater than the number $G = 8$ of the groups. On the other hand, the fairness index is slight influenced by the values of S for all the considered schemes, especially for the pure-NOMA and pure-OMA techniques.

Finally, Tables V and VI report the sum-rate capacity and the fairness index of the considered multiple access schemes for the two different values of the noise figure $F = 16$ dB and $F = 4$ dB, respectively. Compared to the results of Table III, it can be inferred that the noise figure has a negligible impact on the fairness index. On the other hand, as expected, the sum-rate capacity is very sensitive to changes of the noise figure. However, the above conclusions drawn from the comparative analysis carried out with $F = 8$ still hold for such different values of the noise figure.

VII. CONCLUSIONS

In this paper, to ensure high spectral efficiency and massive connectivity in LEO constellations, we have studied the feasibility of superimposing the transmissions of satellites with different Doppler frequency profiles in a NOMA setting. To enhance network fairness, we have developed a theoretical framework that allows one to partition a pool of satellites into groups using orthogonal channel resources, with the goal of achieving high within-group heterogeneity in the Doppler frequency domain such that concurrent transmissions of satellites belonging to the same group can be separated at the sink through MMSE-SIC reception. Our numerical results show that the proposed hybrid NOMA-OMA scheme significantly outperforms existing OMA ones in terms of sum-rate capacity, by exhibiting a better trade-off between rate and fairness than the capacity-achieving pure-NOMA technique. Such a trade-off becomes significant in massive LEO systems, where a fair share of the scarce radio spectrum is one of the main concern.

APPENDIX

THE ECEF COORDINATE SYSTEM

With reference to Fig. 9, the position in the ECEF coordinate system of the n -th satellite belonging to the p -th orbit plane, with $p \in \{1, 2, \dots, P\}$ and $n \in \{1, 2, \dots, N\}$, is defined by the following rotations:

$$\mathbf{r}_{p,n}(t) \triangleq \begin{bmatrix} x_{p,n}(t) \\ y_{p,n}(t) \\ z_{p,n}(t) \end{bmatrix} = (R + h) \mathbf{\Xi}_p \mathbf{\Pi} \mathbf{e}_{p,n}(t) \quad (54)$$

where $\mathbf{e}_{p,n}(t) \triangleq [\cos(\omega t + \gamma_{p,n}), \sin(\omega t + \gamma_{p,n}), 0]^T$,

$$\mathbf{\Pi} \triangleq \begin{bmatrix} \cos \alpha & 0 & -\sin \alpha \\ 0 & 1 & 0 \\ \sin \alpha & 0 & \cos \alpha \end{bmatrix} \quad (55)$$

and

$$\mathbf{\Xi}_p \triangleq \begin{bmatrix} \cos \beta_p & -\sin \beta_p & 0 \\ \sin \beta_p & \cos \beta_p & 0 \\ 0 & 0 & 1 \end{bmatrix} \quad (56)$$

TABLE IV
PARTITION OF THE $L = 19$ SATELLITES WITH FEASIBLE ISLS TOWARDS THE SINK OF THE HYBRID NOMA-OMA SCHEME.

Scheme	Partition
Alg. 1 (opt-DoF/uni-DoF)	$\mathcal{L}_1 = \{1, 9\}, \mathcal{L}_2 = \{2, 4, 11\}, \mathcal{L}_3 = \{3, 6, 12\}, \mathcal{L}_4 = \{5, 10, 13\}, \mathcal{L}_5 = \{7, 17\}, \mathcal{L}_6 = \{8, 14\}, \mathcal{L}_7 = \{15, 19\}, \mathcal{L}_8 = \{16, 18\}$
Alg. 2 (opt-DoF)	$\mathcal{L}_1 = \{1, 3, 6, 7, 8, 11, 19\}, \mathcal{L}_2 = \{2, 12\}, \mathcal{L}_3 = \{13\}, \mathcal{L}_4 = \{5, 14\}, \mathcal{L}_5 = \{10, 15\}, \mathcal{L}_6 = \{16\}, \mathcal{L}_7 = \{17\}, \mathcal{L}_8 = \{4, 9, 18\}$
Alg. 2 (uni-DoF)	$\mathcal{L}_1 = \{6, 11\}, \mathcal{L}_2 = \{1, 12\}, \mathcal{L}_3 = \{9, 13\}, \mathcal{L}_4 = \{3, 14, 19\}, \mathcal{L}_5 = \{4, 8, 15\}, \mathcal{L}_6 = \{7, 16\}, \mathcal{L}_7 = \{10, 17\}, \mathcal{L}_8 = \{2, 5, 18\}$

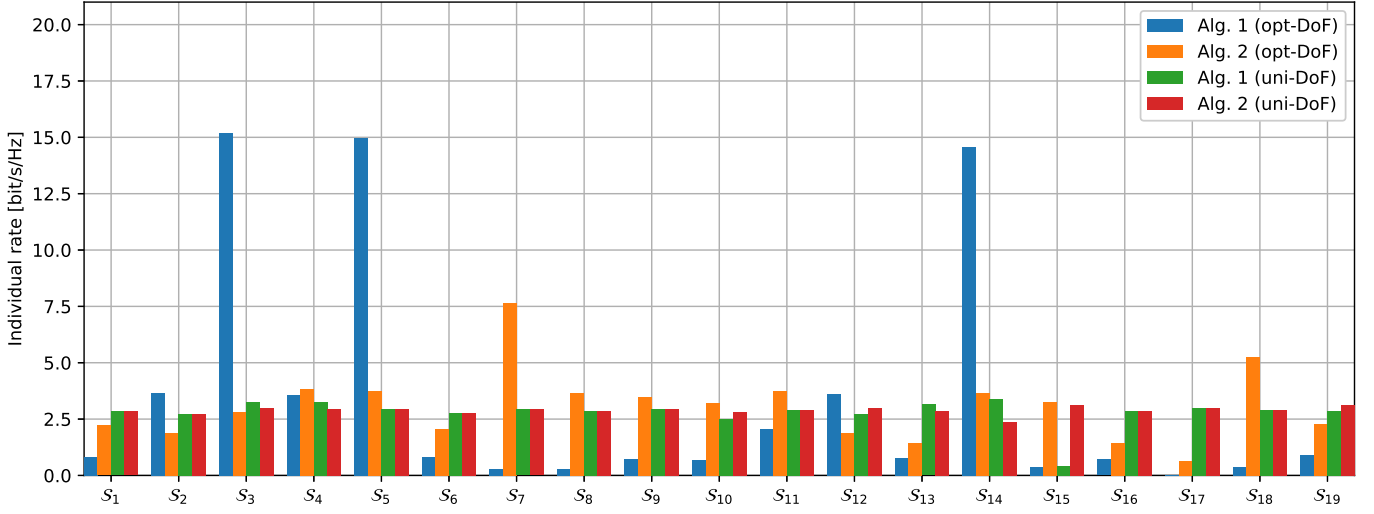


Fig. 6. Individual rates of the $L = 19$ satellites with feasible ISLS towards the sink of the hybrid NOMA-OMA schemes.

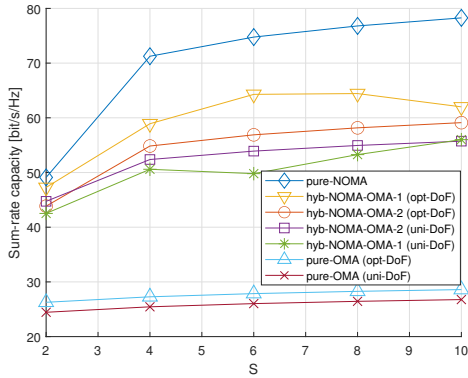


Fig. 7. Sum-rate capacity of the considered schemes as a function of S .

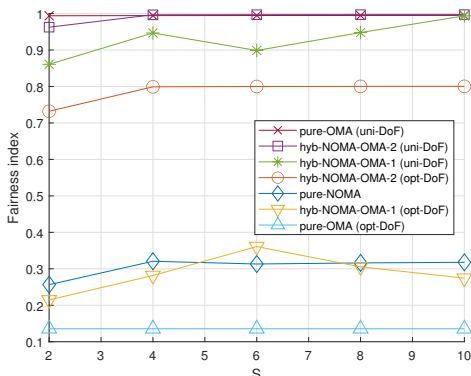


Fig. 8. Fairness index of the considered schemes as a function of S .

TABLE V
SUM-RATE CAPACITY AND FAIRNESS INDEX OF ALL OF THE ANALYZED SCHEMES FOR $F = 16$ dB.

Algorithm	\mathcal{C}_{sum}	\mathcal{F}
pure-NOMA	76.645	0.316
pure-OMA (opt-DoF)	28.237	0.136
pure-OMA (uni-DoF)	23.540	0.994
Alg. 1 (opt-DoF)	68.506	0.250
Alg. 2 (opt-DoF)	58.065	0.800
Alg. 1 (uni-DoF)	46.479	0.946
Alg. 2 (uni-DoF)	48.040	0.996

with

$$\beta_p \triangleq \frac{2\pi(p-1)}{P} \quad (57)$$

$$\gamma_{p,n} \triangleq \frac{2\pi(n-1)}{N} + \frac{2\pi F(p-1)}{K} \quad (58)$$

ω and $\alpha \in [0, \pi/2]$ representing the satellite angular speed and the orbit inclination angle, respectively, and, finally, F is the so-called *phasing* parameter usually designed in order to maximize the minimum distance between satellites [21].

The position can also be represented in spherical coordinates, i.e.,

$$\mathbf{r}_{p,n}(t) = \begin{bmatrix} (R+h) \sin[\theta_{p,n}(t)] \cos[\varphi_{p,n}(t)] \\ (R+h) \sin[\theta_{p,n}(t)] \sin[\varphi_{p,n}(t)] \\ (R+h) \cos[\theta_{p,n}(t)] \end{bmatrix}. \quad (59)$$

REFERENCES

- [1] I. Leyva-Mayorga, B. Soret, M. Röper, D. Wübben, B. Matthiesen, A. Dekorsy, and P. Popovski, "LEO small-satellite constellations for 5G and beyond-5G communications," *IEEE Access*, vol. 8, pp. 184955–184964, 2020.

TABLE VI
SUM-RATE CAPACITY AND FAIRNESS INDEX OF ALL OF THE ANALYZED
SCHEMES FOR $F = 4$ DB.

Algorithm	\mathcal{C}_{sum}	\mathcal{F}
pure-NOMA	84.016	0.321
pure-OMA (opt-DoF)	30.049	0.136
pure-OMA (uni-DoF)	28.222	0.995
Alg. 1 (opt-DoF)	73.891	0.251
Alg. 2 (opt-DoF)	63.036	0.800
Alg. 1 (uni-DoF)	56.703	0.954
Alg. 2 (uni-DoF)	59.160	0.997

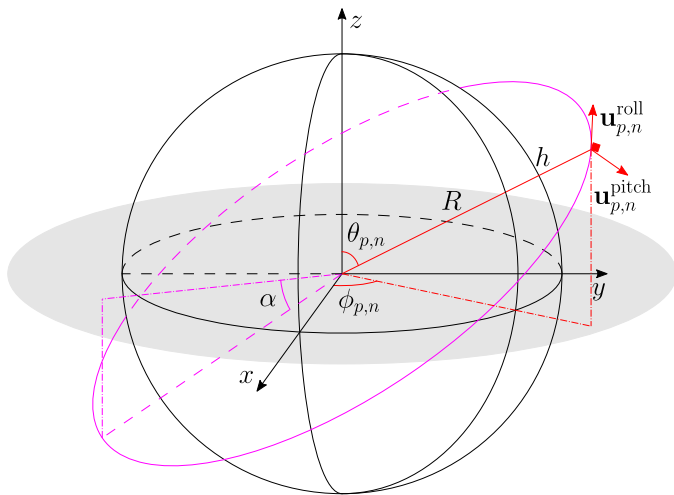


Fig. 9. The ECEF coordinate system. Both Cartesian and spherical coordinates are highlighted in the picture.

- [2] T. Darwish, G. K. Kurt, H. Yanikomeroglu, M. Bellemare, and G. Lamontagne, "LEO satellites in 5G and beyond networks: A review from a standardization perspective," *IEEE Access*, vol. 10, pp. 35 040–35 060, 2022.
- [3] J. Chu, X. Chen, C. Zhong, and Z. Zhang, "Robust design for NOMA-based multibeam LEO satellite Internet of Things," *IEEE Internet of Things Journal*, vol. 8, no. 3, pp. 1959–1970, 2021.
- [4] A. U. Chaudhry and H. Yanikomeroglu, "Free space optics for next-generation satellite networks," *IEEE Consumer Electronics Magazine*, vol. 10, no. 6, pp. 21–31, 2021.
- [5] —, "Laser intersatellite links in a starlink constellation: A classification and analysis," *IEEE Vehicular Technology Magazine*, vol. 16, no. 2, pp. 48–56, 2021.
- [6] H. Al-Hraishawi, H. Chougrani, S. Kisseleff, E. Lagunas, and S. Chatzinotas, "A survey on nongeostationary satellite systems: The communication perspective," *IEEE Communications Surveys & Tutorials*, vol. 25, no. 1, pp. 101–132, 2023.
- [7] I. Leyva-Mayorga, B. Soret, M. Röper, D. Wübben, B. Matthiesen, A. Dekorsy, and P. Popovski, "LEO small-satellite constellations for 5G and beyond-5G communications," *IEEE Access*, vol. 8, pp. 184 955–184 964, 2020.
- [8] S. Nie and I. F. Akyildiz, "Channel modeling and analysis of inter-small-satellite links in terahertz band space networks," *IEEE Transactions on Communications*, vol. 69, no. 12, pp. 8585–8599, 2021.
- [9] I. Leyva-Mayorga, B. Soret, and P. Popovski, "Inter-plane inter-satellite connectivity in dense LEO constellations," *IEEE Transactions on Wireless Communications*, vol. 20, pp. 3430–3443, 2021.
- [10] S. M. R. Islam, N. Avazov, O. A. Dobre, and K.-s. Kwak, "Power-domain non-orthogonal multiple access (NOMA) in 5G systems: Potentials and challenges," *IEEE Communications Surveys & Tutorials*, vol. 19, no. 2, pp. 721–742, 2017.
- [11] W. Shin, M. Vaezi, B. Lee, D. J. Love, J. Lee, and H. V. Poor, "Non-orthogonal multiple access in multi-cell networks: Theory, performance, and practical challenges," *IEEE Communications Magazine*, vol. 55, no. 10, pp. 176–183, 2017.
- [12] Z. Yin, M. Jia, W. Wang, N. Cheng, F. Lyu, Q. Guo, and X. Shen, "Secrecy rate analysis of satellite communications with frequency domain NOMA," *IEEE Transactions on Vehicular Technology*, vol. 68, no. 12, pp. 11 847–11 858, 2019.
- [13] Z. Yin, N. Cheng, Y. Hui, W. Wang, L. Zhao, K. Aldubaikhy, and A. Alqasir, "Multi-domain resource multiplexing based secure transmission for satellite-assisted IoT: AO-SCA approach," *IEEE Transactions on Wireless Communications*, vol. 22, no. 11, pp. 7319–7330, 2023.
- [14] J. Pi, Y. Ran, H. Wang, Y. Zhao, R. Zhao, and J. Luo, "Dynamic planning of inter-plane inter-satellite links in LEO satellite networks," in *ICC 2022 - IEEE International Conference on Communications*, 2022, pp. 3070–3075.
- [15] X. Yan, K. An, T. Liang, G. Zheng, Z. Ding, S. Chatzinotas, and Y. Liu, "The application of power-domain non-orthogonal multiple access in satellite communication networks," *IEEE Access*, vol. 7, pp. 63 531–63 539, 2019.
- [16] Z. Gao, A. Liu, and X. Liang, "The performance analysis of downlink NOMA in LEO satellite communication system," *IEEE Access*, vol. 8, pp. 93 723–93 732, 2020.
- [17] Z. Gao, A. Liu, C. Han, and X. Liang, "Sum rate maximization of massive MIMO NOMA in LEO satellite communication system," *IEEE Wireless Communications Letters*, vol. 10, no. 8, pp. 1667–1671, 2021.
- [18] R. Ge, D. Bian, J. Cheng, K. An, J. Hu, and G. Li, "Joint user pairing and power allocation for NOMA-based GEO and LEO satellite network," *IEEE Access*, vol. 9, pp. 93 255–93 266, 2021.
- [19] W. Tachikawa, K. Yoshii, and S. Shimamoto, "Performance analysis of uplink and downlink NOMA system in inter-satellite networks," in *ICC 2021 - IEEE International Conference on Communications*, 2021, pp. 1–6.
- [20] Q. Hu, J. Jiao, Y. Wang, S. Wu, R. Lu, and Q. Zhang, "Multitype services coexistence in uplink NOMA for dual-layer LEO satellite constellation," *IEEE Internet of Things Journal*, vol. 10, no. 3, pp. 2693–2707, 2023.
- [21] J. Liang, A. U. Chaudhry, and H. Yanikomeroglu, "Phasing parameter analysis for satellite collision avoidance in Starlink and Kuiper constellations," in *2021 IEEE 4th 5G World Forum (5GWF)*, 2021, pp. 493–498.
- [22] M. Civas and O. B. Akan, "Terahertz wireless communications in space," 2021. [Online]. Available: <https://arxiv.org/abs/2110.00781>
- [23] D. Tse and P. Viswanath, *Fundamentals of Wireless Communication*. USA: Cambridge University Press, 2005.
- [24] A. Napolitano, *Generalizations of Cyclostationary Signal Processing: Spectral Analysis and Application*. John Wiley & Sons, Ltd. – IEEE Press, 2012.
- [25] 3GPP, "3rd Generation Partnership Project; Technical Specification Group Radio Access Network; Study on New Radio (NR) to Support Non Terrestrial Networks (Release 15)," 3rd Generation Partnership Project (3GPP), Technical Report (TR) 38.811, 09 2019, version 15.2.0.
- [26] J. G. Proakis, *Digital Communications*, 5th ed. McGraw Hill, 2007.
- [27] P. Li, D. Paul, R. Narasimhan, and J. Cioffi, "On the distribution of SINR for the MMSE MIMO receiver and performance analysis," *IEEE Transactions on Information Theory*, vol. 52, pp. 271–286, 2006.
- [28] B. D. and G. R., *Data Networks*. Englewood Cliffs: Prentice-Hall, 2001.
- [29] R. A. Horn and C. R. Johnson, *Matrix analysis*. Cambridge university press, 2012.
- [30] J. Bellorado, S. Ghassemzadeh, and A. Kavcic, "Approaching the capacity of the MIMO Rayleigh flat-fading channel with QAM constellations, independent across antennas and dimensions," *IEEE Transactions on Wireless Communications*, vol. 5, no. 6, pp. 1322–1332, 2006.
- [31] V. Vahid, "Set partition principles," in *Transactions of the ninth Prague conference on information theory, statistical decision functions, and random processes (Prague, 1982)*, 1983, pp. 251–256.
- [32] —, "Set partition principles revisited," in *Advances in Pattern Recognition: Joint IAPR International Workshops SSPR'98 and SPR'98 Sydney, Australia, August 11–13, 1998 Proceedings*. Springer, 1998, pp. 875–881.
- [33] H. Späth, "Anticlustering: Maximizing the variance criterion," *Control and Cybernetics*, vol. 15, no. 2, pp. 213–218, 1986.
- [34] M. Papenberg and G. W. Klau, "Using anticlustering to partition data sets into equivalent parts," *Psychological Methods*, vol. 26, no. 2, pp. 161–174, apr 2021.
- [35] R. Jain, D.-M. Chiu, and W. Hawe, "A quantitative measure of fairness and discrimination for resource allocation in shared computer systems," *CoRR*, vol. cs.NI/9809099, 1998.
- [36] D. Karapetyan, S. Mitrovic Minic, K. T. Malladi, and A. P. Punnen, "Satellite downlink scheduling problem: A case study," *Omega*, vol. 53, pp. 115–123, 2015.
- [37] J. Yan, L. Xing, P. Wang, L. Sun, and Y. Chen, "A scheduling strategy to inter-satellite links assignment in GNSS," *Advances in Space Research*, vol. 67, no. 1, pp. 198–208, 2021.

- [38] M. Roth, H. Brandt, and H. Bischl, "Implementation of a geographical routing scheme for low Earth orbiting satellite constellations using intersatellite links," *International Journal of Satellite Communications and Networking*, vol. 39, no. 1, pp. 92–107, 2021.



Donatella Darsena (Senior Member, IEEE) received the Dr. Eng. degree *summa cum laude* in telecommunications engineering in 2001, and the Ph.D. degree in electronic and telecommunications engineering in 2005, both from the University of Napoli Federico II, Italy. From 2001 to 2002, she worked as embedded system designer in the Telecommunications, Peripherals and Automotive Group, STMicroelectronics, Milano, Italy. In 2005 she joined the Department of Engineering at Parthenope University of Napoli, Italy and worked first as an Assistant Professor and then as an Associate Professor from 2005 to 2022. She is currently an Associate Professor in the Department of Electrical Engineering and Information Technology of the University of Napoli Federico II, Italy. Her research interests are in the broad area of signal processing for communications, with current emphasis on reflected-power communications, orthogonal and nonorthogonal multiple access techniques, wireless system optimization, and physical-layer security. Dr. Darsena has served as a Senior Editor for IEEE ACCESS since 2024, Executive Editor for IEEE COMMUNICATIONS LETTERS since 2023, and Associate Editor for IEEE SIGNAL PROCESSING LETTERS since 2020. She was an Associate Editor of IEEE ACCESS (from 2018 to 2023), of IEEE COMMUNICATIONS LETTERS (from 2016 to 2019), and Senior Area Editor of IEEE COMMUNICATIONS LETTERS (from 2020 to 2023).



Giacinto Gelli (Senior Member, IEEE) received the Dr. Eng. degree *summa cum laude* in electronic engineering in 1990, and the Ph.D. degree in computer science and electronic engineering in 1994, both from the University of Napoli Federico II. From 1994 to 1998, he was an Assistant Professor with the Department of Information Engineering, Second University of Napoli. Since 1998 he has been with the Department of Electrical Engineering and Information Technology, University of Napoli Federico II, first as an Associate Professor, and since November 2006 as a Full Professor of telecommunications. He also held teaching positions at the University of Napoli Parthenope. His research interests are in the broad area of signal and array processing for communications, with current emphasis on reflected-power communication systems, multicarrier modulation systems, and space-time techniques for cooperative and cognitive communications systems.



Ivan Iudice received the B.S. and M.S. degrees in telecommunications engineering in 2008 and 2010, respectively, and the Ph.D. degree in information technology and electrical engineering in 2017, all from University of Napoli Federico II, Italy. Since November 2011, he has been with the Italian Aerospace Research Centre (CIRA), Capua, Italy. He first served as part of the Electronics and Communications Laboratory and he is currently part of the Security Unit. He is involved in several international projects. He serves as reviewer for several international journals and as TPC member for several international conferences. He is author of several papers on refereed journals and international conferences. His research activities mainly lie in the area of signal and array processing for communications, with current interests focused on physical-layer security, space-time techniques for cooperative communications systems and reconfigurable metasurfaces.



Francesco Verde (Senior Member, IEEE) received the Dr. Eng. degree *summa cum laude* in electronic engineering from the Second University of Napoli, Italy, in 1998, and the Ph.D. degree in information engineering from the University of Napoli Federico II, in 2002. Since December 2002, he has been with the University of Napoli Federico II, Italy. He first served as an Assistant Professor of signal theory and mobile communications and, since December 2011, he has served as an Associate Professor of telecommunications with the Department of Electrical Engineering and Information Technology. His research activities include reflected-power communications, orthogonal/non-orthogonal multiple-access techniques, wireless systems optimization, and physical-layer security. Prof. Verde has been involved in several technical program committees of major IEEE conferences in signal processing and wireless communications. He has served as Associate Editor for IEEE TRANSACTIONS ON VEHICULAR TECHNOLOGY since 2022. He was an Associate Editor of the IEEE TRANSACTIONS ON SIGNAL PROCESSING (from 2010 to 2014), IEEE SIGNAL PROCESSING LETTERS (from 2014 to 2018), IEEE TRANSACTIONS ON COMMUNICATIONS (from 2017 to 2022), and Senior Area Editor of the IEEE SIGNAL PROCESSING LETTERS (from 2018 to 2023), as well as Guest Editor of the EURASIP Journal on Advances in Signal Processing in 2010 and SENSORS MDPI in 2018-2022.